Evolution of continental temperature seasonality from the Eocene greenhouse to the Oligocene icehouse - A model-data comparison

Agathe Toumoulin[1], Delphine Tardif[1,2], Yannick Donnadieu[1], Alexis Licht[1], Jean-Baptiste Ladant[3], Lutz Kunzmann[4], Guillaume Dupont-Nivet[5,6]

[1]Aix Marseille Université, CNRS, IRD, INRA, Collège de France, CEREGE, 13545 Aix-en-Provence, France
[2]Université de Paris, Institut de physique du globe de Paris, CNRS, F-75005 Paris, France
[3]Laboratoire des Sciences du Climat et de l'Environnement, LSCE/IPSL, CEA-CNRS-UVSQ, Université Paris-Saclay, 91191 Gif-sur-Yvette, France
[4]Senckenberg Natural History Collections Dresden, Königsbrücker Landstraße 159, 01109 Dresden, Germany
[5]Géosciences Rennes, UMR CNRS 6118, Univ Rennes, 35042 Rennes, France
[6]Institute of Geosciences, Potsdam University, 14469 Potsdam, Germany

Correspondence to: Agathe Toumoulin (agathe.toumoulin@gmail.com)

Abstract. At the junction of greenhouse and icehouse climate states, the Eocene-Oligocene Transition (EOT) is a key moment in Cenozoic climate history. While it is associated with severe extinctions and biodiversity turnovers on land, the role of terrestrial climate evolution remains poorly resolved, especially the associated changes in seasonality. Some paleobotanical and geochemical continental records in parts of the Northern Hemisphere suggest the EOT is associated with a marked cooling in winter, leading to the development of more pronounced seasons (i.e., increase of the Mean Annual Range of Temperature, MATR). However, the MATR increase has been barely studied by climate models and large uncertainties remain on its origin, geographical extent and impact. In order to better understand and describe temperature seasonality changes between the middle Eocene and the early Oligocene, we use the Earth System Model IPSL-CM5A2 and a set of simulations reconstructing the EOT through three major climate forcings: pCO_2 decrease (1120, 840 and 560 ppm), the Antarctic ice-sheet (AIS) formation, and the associated sea-level decrease. Our simulations suggest that pCO_2 lowering alone is not sufficient to explain the seasonality evolution described by the data through the EOT, but rather that the combined effects of pCO_2, AIS formation, and increased continentality provide the best data-model agreement. pCO_2 decrease induces a zonal pattern with alternating increasing and decreasing seasonality bands particularly strong in the northern high-latitudes (up to 8°C MATR increase) due to sea-ice and surface albedo feedback. Conversely, the onset of the AIS is responsible for a more constant surface albedo yearly, which leads to a strong decrease in seasonality in the southern mid- to high-latitudes (> 40°S). Finally, continental areas emerged due to the sea level lowering cause the largest increase in seasonality and explain most of the global heterogeneity in MATR changes (ΔMATR) patterns. ΔMATR patterns we reconstruct are generally consistent with the variability of the EOT biotic crisis intensity across the Northern Hemisphere and provide insights on their underlying mechanisms.

1 Introduction

1.1 Context and aim of the study

The Eocene-Oligocene Transition (EOT) is marked by an abrupt cooling event (~2.9°C from marine proxies; Hutchinson et al., 2021), considered as the hinge between the Eocene greenhouse and the later Cenozoic icehouse. This event is associated with the first major expansion of the Antarctic ice-sheet with an estimated sea level drop of ~70 m (Hutchinson et al., 2021; Miller et al., 2020). The EOT is described as a relatively brief event (~790 000 years), with two successive steps (at ca. 33.9 and 33.7) recognized in extensively studied marine environments, especially from deep ocean $\delta^{18}O$ values (e.g. Katz et al., 2008; Zachos et al., 2001; see the review of Hutchinson et al., 2021).

Reported vegetation responses to the EOT appear heterogeneous across continents with important composition changes in some areas (e.g., West Coast of the United States, Greenland, Asia), notably where faunal turnover is important (e.g. Barbolini et al., 2020; Eldrett et al., 2009; Hutchinson et al., 2021; Pound and Salzmann, 2017; Wolfe, 1994). A number of paleobotanical and geochemical studies consistently suggest that the decrease in continental temperatures was particularly marked during winter months, thus leading to higher seasonal temperature contrasts, which are designated as a potential driving mechanism for biotic turnovers (e.g. Eldrett et al., 2011; Mosbrugger et al., 2005; Page et al., 2020; Utescher et al., 2015; Zanazzi et al., 2015). Evoked forcing mechanisms explaining this enhanced winter cooling are pCO_2, AIS inception, and increased continentality, although it remains difficult to quantify and disentangle their respective contribution from field data only. Understanding the drivers of these seasonal changes is thus important, not only for assessing the climate system behaviour under major pCO_2 variations, but also to better describe the paleoenvironmental context associated with major extinction events of the EOT such as the "Grande Coupure" in Europe and the "Mongolian Remodelling" in central Asia (Meng and McKenna, 1998; Stehlin, 1909; see Coxall and Pearson, 2007 for a review).

By comparing paleoclimate simulations to a synthesis of indicators of seasonality changes (Table S1), our study attempts to reconstruct the evolution of seasonal temperature contrast from the middle Eocene to the early Oligocene. The EOT is broken down into five simulations, describing the evolution of three major forcing at that time: the pCO_2 drawdown, the AIS expansion and the resulting sea-level lowering, in order to understand the respective contribution of each component on the resulting seasonality change patterns, along with their possible synergies and retroactions.

1.2 Temperature seasonality and its evolution

Temperature seasonality can be quantified by the Mean Annual Temperature Range (MATR), which consists in the temperature difference between the warmest and coldest months of the year. Increasing MATR can occur through increased summer temperatures, lowered winter temperatures, or both. MATR is practical because it can be directly calculated from temperature proxies providing an estimation of the lowest and highest temperatures within a year. This is the case for the Climate Leaf Analysis Multivariate Program (CLAMP), which reconstructs temperatures from the modern correlation between climate variables and leaf physiognomy (Wolfe, 1993; Yang et al., 2011), or the Coexistence Approach (CA), which uses

modern relatives of fossil species to define a mutual climate range of environmental characteristics (Grimm and Potts, 2016; Mosbrugger and Utescher, 1997; Utescher et al., 2014). MATR can also be deduced from the variability of the temperature signal in geochemical proxies for temperatures, stable oxygen isotopes ($\delta^{18}O$), as the time resolution of the proxy does rarely allow for the direct reconstruction of seasonal temperatures (e.g. Ivany et al., 2000; Wade et al., 2012).

The spatial distribution of temperature seasonality changes across the EOT appear heterogeneous in proxy data (e.g. Pound and Salzmann, 2017). Most changes are described in the Northern Hemisphere from paleobotanical reconstructions, and converge to show seasonalities stronger in the early Oligocene than in the mid- to late Eocene. In North America, Western and central Europe, seasonality increase is recorded by the decline of species characteristic of warm paratropical to temperate environments such as palms (e.g., *Nypa* sp.), plants from myrtle and eucalyptus family (Myrtaceae, e.g., *Rhodomyrtophyllum* sp.), conifers (e.g., *Doliostrobus sp.*) and some plant families with tropical elements (e.g., Annonaceae, Lauraceae, Cornaceae, Icacinaceae, Menispermaceae), and, depending on the bioclimatic zones, the expansion of temperate to boreal vegetation through the increase of deciduous and / or coniferous species (Eldrett et al., 2009; Kunzmann et al., 2016; Kvaček, 2010; Kvaček et al., 2014; Mosbrugger et al., 2005; Utescher et al., 2015; Wolfe, 1992). These vegetation changes are associated with a decrease of the Coldest Month Mean Temperatures (CMMT) across the EOT and start before the EOT at some localities, during the mid- to late Eocene (Eldrett et al., 2009; Moraweck et al., 2019; Mosbrugger et al., 2005; Tanrattana et al., 2020; Tosal et al., 2019; Utescher et al., 2015; Wolfe, 1994). Isotopic analyses have documented this seasonality increase in different continental localities between the Priabonian (37.8 to 33.9 Ma) and the Rupelian (33.9 to 27.82 Ma; Grimes et al., 2005; Hren et al., 2013; Zanazzi et al., 2015). While some of the changes are not directly quantifiable (e.g., the reduction of gastropods growing season length, United Kingdom; Hren et al., 2013; dental morphological changes for grazing perissodactyls, Europe; Joomun et al., 2010), others can demonstrate strong MATR increase (e.g., amplified by 15.6°C, Canada; Zanazzi et al., 2015). Temperature seasonality increase is also documented for shallow waters of the Gulf of Mexico (increase of the MATR; Ivany et al., 2000; Wade et al., 2012). Some studies have suggested a link between increased temperature seasonality and latitude (e.g., Eldrett et al., 2009; Zanazzi et al., 2007, 2015) but data seem insufficient to validate this relationship and this trend has not been confirmed by recent palynological compilation (Pound and Salzmann, 2017).

Data from southeast Europe and Anatolia show generally weaker and heterogeneous changes in temperature seasonality, with either no seasonality changes, slight seasonality lowering or slight seasonality strengthening from the mid-Eocene to the Rupelian (Bozukov et al., 2009; Kayseri-Özer, 2013). This variability has been explained by a strong marine influence on this part of Eocene Europe (Kayseri-Özer, 2013). Conversely, North and East Asia temperature seasonality evolution is more comparable to western Europe and North America trends (Quan et al., 2012; Utescher et al., 2015). Vegetation changes reflect an increase of the seasonal temperature range, mainly through the EOT (MATR increase of 2 to 2.5°C; CMMT decrease of ~2.2°C, Quan et al., 2012; Utescher et al., 2015). The appearance of tubers in lotus (*Nelumbo* sp.) during the Eocene suggests the establishment of a dormant phase in these plants and thus, of a period unfavorable to plant growth (Li et al., 2014). Fossils showing these structures have been described in Southern China (Hainan Province) and easternmost Russia (Kamchatka

Peninsula) leading to hypothesize they could be favored by cooling and increased seasonality on the East Asian continent during the Eocene (Budantsev, 1997; Li et al., 2014).

In the Southern Hemisphere, studies of Paleogene localities are rarer. Despite a record of late Eocene cooling in Australia, New Zealand and Patagonia, independent proxies (stable isotopes on teeth, bones and pedogenic carbonates, paleobotanical reconstructions) do not suggest a marked temperature seasonality during the Eocene (Cowlyn and Hren, 2019; Kohn et al., 2015; Laurenato et al., 2021; Nott and Owen, 1992; Pocknall, 1989). In Australia, the presence of more pronounced wood rings suggests a late Paleogene increase in seasonality starting in the mid-Oligocene at the earliest (Bishop and Bamber, 1985; Nott and Owen, 1992). Finally, the environmental and climatic impact of the EOT in continental Africa remains poorly documented (Hutchinson et al., 2021; Saarinen et al., 2020).

1.3 Former model work

Different modelling studies have illustrated the priming role of pCO$_2$ lowering during the EOT, but most focused on oceans through mean annual temperature changes (Baatsen et al., 2020; Goldner et al., 2014; Hutchinson et al., 2018, *see* 2020; Kennedy et al., 2015; Kennedy-Asser et al., 2019, 2020; Ladant et al., 2014b). The model intercomparison study of Hutchinson et al. (2021) has shown a reasonable agreement between 4X to 2X (i.e., 1120 and 560 ppm respectively) modelling experiments and proxy-data atmospheric and surface ocean temperature reconstructions from the late Eocene and the early Oligocene, respectively. They show, however, that changes in EOT SSTs were on average best represented by a pCO$_2$ shift from 910 ppm to 560 ppm (i.e., a drop of 1.6X). In addition, a recent model-data study of Laurenato et al. (2021) explored Australia climate evolution through the EOT, and estimated a pCO$_2$ drop ranging 260 – 380 ppm (drop of ~ 0.9 – 1.3X). A first attempt to explain temperature seasonality change across the EOT was made by Eldrett et al. (2009). In their palynological and modelling study, Eldrett and coauthors explained high latitude (Greenland) seasonality strengthening by pCO$_2$ drop and the consequent increase of sea-ice formation over the Arctic Ocean. In their experiment, sea-ice extension induces a strong albedo feedback, which results in a large decrease of atmospheric temperature during winter. Additionally, changes in geography (topography, land-sea distribution) may have significant effects on terrestrial temperatures at a regional scale (e.g., Lunt et al., 2016; Li et al., 2018). EOT modelling experiments yield mixed answers regarding the temperature feedback resulting from both AIS and contemporary paleogeographic changes (opening of Southern Ocean gateways, Antarctic geography or global geography; Goldner et al., 2014; Hutchinson et al., 2021; Kennedy et al., 2015; Ladant et al., 2014a, 2014b). The few studies testing the combined effect of both AIS and paleogeographic changes (Kennedy et al., 2015; Laurenato et al., 2021) suggested a moderate impact of AIS on global climate sensitivity, as previously suggested by other modelling work (Goldner et al., 2013; Kennedy et al., 2015).

2 Material and methods

2.1 Model and simulation setting

We used the IPSL-CM5A2 general circulation model, which is built upon the CMIP5 Earth system model developed at the Institut Pierre-Simon Laplace (IPSL), IPSL-CM5A-LR (Dufresne *et al.*, 2013, Sepulchre et al., 2019). The IPSL-CM5A-LR Earth system model is composed of the LMDZ atmospheric model (Hourdin *et al.*, 2013), the ORCHIDEE land surface and vegetation model (Krinner *et al.*, 2005), and the NEMO v3.6 ocean model which includes modules for ocean dynamics (OPA8.2, Madec, 2008), biochemistry (PISCES, Aumont *et al.* 2015) and sea-ice (LIM2, Fichefet and Morales-Maqueda, 1997). The atmospheric grid has a horizontal resolution of 3.75° longitude per 1.875° latitude (96 × 95 grid points), and is divided into 39 vertical levels. For a more detailed description of the model and its different components, the reader is referred to Sepulchre *et al.* (2020).

Five simulations were carried out to reconstruct the evolution of temperature seasonality from the middle Eocene to the early Oligocene (Table 1). The applied 40 Ma paleogeography framework is the map developed by Poblete et al. (2021) and already used in Tardif et al. (2020) and Toumoulin et al. (2020). It features common late Eocene geography characteristics such as: an open Panama Seaway, an open Tethys with submerged Arabian Peninsula, a strongly maritime Europe, a Turgai land bridge connecting Northern Europe with Asia, and narrow Southern Ocean gateways (Figure 1). The orbital parameters were set to preindustrial values and the solar constant was reduced accordingly to its Eocene value (1360.19 W/m^2; Gough, 1981). Vegetation was implemented as a boundary condition, using a zonal band of PFTs using modern vegetation distribution patterns.

Simulations were compared in pairs to highlight differences between the middle/late Eocene and the early Oligocene. The simulation set is composed of both realistic and idealized experiments (Table 1). Simulations 4X, 3X and 2X represent most of the pCO$_2$ range described from the mid-Eocene (Lutetian) to the early Oligocene (Rupelian; Foster et al., 2017). These pCO$_2$ values enable the description of the pCO$_2$ reduction effect on climate through this time interval and have been used in most former modelling experiments on the EOT (Hutchinson et al., 2021). Simulations 4X and 3X cover the range of potential climate values prior to the EOT (Lutetian to Priabonian). The idealized simulation 2X allows the identification of a 1 to 2 PAL (Preindustrial Atmospheric Levels, 1PAL = 280 ppm) pCO$_2$ lowering alone. In a complementary way, simulations 2X-ICE and 2X-ICE-SL describe the early Oligocene climate, following the Antarctic Ice-sheet formation. Both simulations are parameterized in the same way apart from the sea level, which is 70 m lower in 2X-ICE-SL. The use of 2X-ICE provides a theoretical description of the effect of an ice-covered Antarctica on climate, while 2X-ICE-SL constitutes a realistic representation of the early Oligocene climate. In these experiments, the Antarctic ice cap was set to 32.5.10^6 km^3 according to Ladant et al. (2014b). The 70-m sea-level drop was defined following eustatic drop estimates for the EOT (Coxall et al., 2005; Katz et al., 2008; Lear et al., 2008; Miller et al., 2020). It is responsible for important geography changes related to an increase of land proportion, such as the emergence of the Arabian Peninsula and the retreat of the proto-Paratethys epicontinental sea.

All simulations run for 4000 years until temperatures indicate a quasi-equilibrium with only negligible temperature drift within the global mean ocean (< 0.1°C/century; Figure S1). These trends are consistent with most model studies and do not affect the quality of atmospheric change described in this study (e.g. Hutchinson et al., 2018; Lunt et al., 2016). The results considered here are averages of the last 100 years of the model runs.

2.2 Data compilation

Simulation results were compared to MATR changes (ΔMATR) documented by proxy-data records (Table S1). We compiled published MATR and CMMT proxy-data from various research fields: paleobotany (macrofossils and palynology), geochemistry (isotopic measurements on various material), and paleontology. The data were selected to range from the Lutetian (47.8 Ma) to the end of the Rupelian (27.8 Ma). This large time interval allows the representation of seasonal temperature changes parallel to the long-term cooling of the Eocene. The inclusion of data from the middle Eocene allows a comparison with simulations testing the effect of a pCO$_2$ lowering alone, before AIS formation at the EOT. It is justified by the presence of paleobotanical records suggesting a strengthening of the seasons already from the Lutetian to the Priabonian (e.g. Li et al., 2014; Mosbrugger et al., 2005). Compiled Eocene-Oligocene ΔMATR correspond either to the values given in original publications, when they were available and precise, or to values re-calculated from the original data. For publications for which ΔMATR were recalculated, we proceeded by grouping the closest sites (especially in terms of latitudes) and checked that the values obtained were consistent with the authors original interpretation of the paleoenvironmental context. Half of the data come from the pollen compilation of Pound and Salzmann (2017). A selection was made through this study data to keep (1) the best dated samples, according to their dating quality indicator (data Q1 to Q3; Pound and Salzmann, 2017), and (2) sites with temperature estimates for the Priabonian and Rupelian, or at least one nearby locality that could be compared. No Eocene-Oligocene site was selected for more clarity. In an effort to limit the addition of overly uncertain ΔMATR data, sites with a range of CMMT estimates (CMMTmax - CMMTmin) ≥ 10°C (either for Priabonian or Rupelian sites) were excluded. Some previously published seasonality increases were not here associated with estimate of ΔMATR, because they were either (1) suggested from other parameters, such as the length of the growing season, which does not allow the calculation of the MATR (Hren et al., 2013), or (2) derived from qualitative data that cannot be specifically associated with temperature values (e.g., organism morphological changes such as teeth shape or plant tuber appearance; Joomun et al., 2010; Li et al., 2014). These sites are displayed on the maps, but are not included in quantitative analyses (section 2.3). In order to better estimate the impact of changes in temperature seasonality, the length of the plant growing season (i.e., the number of months with an average temperature above 10°C) was recalculated using the formula of Grein et al., (2013) for coexistence approach data (Table 1). Paleocoordinates for every locality were reconstructed using an online service of *Gplates*, according to the 40 Ma paleogeography used for the paleoclimate models (Poblete et al., 2021) that essentially follows the plate tectonic reconstruction models of Matthews et al. (2016) with some modifications.

2.3 Comparison of model and data ∆MATR

190   Different analyses were made to evaluate the data-model agreement for temperature seasonality changes from the Priabonian to Rupelian (Table 2). Modelled ∆MATR values were extracted from a 3° longitude by 3° latitude area surrounding each data locality. First, a general agreement percentage was calculated from the direction of seasonality changes alone to assert the agreement between our simulation and qualitative data. For this metric, model predictions are considered "good" for an individual site if modelled ∆MATR changes in the same direction as the data (i.e., if modelled ∆MATR increase/decrease at

195   the location of a data point showing seasonality increase/decrease). For data indicating null ∆MATR, a good agreement was considered with model values ranging from - 0.5 to 0.5°C.

In addition, Priabonian to Rupelian seasonality changes were compared to model predictions, by (1) assessing their correlation and (2) calculating the root of the mean squared distance between their values. These two analyses were performed using R (version 4.0.3; R CoreTeam, 2020, Boston, USA). Given the limited number of quantitative Priabonian–Rupelian data (n

200   = 29), the statistical correlation of data-model ∆MATR was assessed from average ∆MATR with the non-parametric Spearman rank test. In this analysis, we used the common significance level, α, of 0.05 (i.e., *p-values* < 0.05 indicate significant correlations). Data-model agreement was also assessed through the Root Mean Squared Estimate, which consists in calculating the root of the mean squared distance between model and data values for comparable points (RMSE, see Kennedy-Asser et al., 2020, and their Figure S1 for a detailed presentation of the method). Conversely to the Spearman Rank Test for which

205   mean ∆MATR estimations were used, the distance is here measured using the full range of estimates at each data locality (i.e., minimum and maximum ∆MATR). Note that, because it considers the full range of ∆MATR, this method tends to minimize the difference between model and data. The lower bound of modelled ∆MATR at each locality was calculated as the difference between the lowest MATR value over the 3° x 3° area centred around the locality for an Oligocene-like cold simulation (2X, 2X-ICE or 2X-ICE-SL) and the highest MATR value over the 3° x 3° area for an Eocene simulation (4X or 3X). For the upper

210   bound, we used the difference between the higher MATR value over the same area for an Oligocene-like cold simulation and the lower MATR value for an Eocene simulation.

The RMSE adjusted to ∆MATR is written as follows:

$$\text{RMSE}_{(MATR\text{-}changes)} = \text{SQRT} ((\cdot(MATR_{(diff\text{-}data)} - MATR_{(diff\text{-}model)})^2/n) \qquad (1)$$

Where *MATR$_{diff\text{-}data}$* and *MATR$_{diff\text{-}model}$* are MATR Priabonian to Rupelian changes estimated by data and model respectively,

215   and *n* the total number of localities.

3 Results

3.1 Simulated response to *p*CO$_2$ lowering

In this section, we compare the simulations 4X, 3X, 2X together to describe the effects of *p*CO$_2$ drawdown on climate and provide a range of possible MAT and MATR change intensities. The simulation pair 2X-4X represents the strongest possible

changes, 3X-4X the weakest changes, and 2X-3X an intermediate scenario (see section 2.1). Mean annual temperatures decrease strongly in our different experiments (Table 1, Figure 2). The halving of pCO$_2$ from 4X to 2X alone (i.e., without AIS formation and sea level drop) induces a global cooling of 5.8°C and 5.0°C for the air temperature and the surface ocean respectively (Table 1). A pCO$_2$ drop of 1 PAL induces a 2.7 to 3.1°C lowering of MAT and a 2.3 to 2.7°C cooling of the SST, for 4X to 3X and 3X to 2X changes, respectively. Along with its effect on annual temperatures and regardless of its intensity, pCO$_2$ decrease induces zonal ΔMATR including (1) an increase of MATR at high-latitudes (especially in the North), (2) a decrease of MATR across most mid-latitudes, and (3) moderate changes at low-latitudes, which we detail in the following sections 3.1.2 and 3.1.3 (for Eocene MATR values see Figure S2).

3.1.2 Areas with increased seasonality

Temperature changes are characterized by polar amplification, with a stronger winter cooling at high-latitudes (Figure 2. a,b,e,f,i,j), likely due to the combined effect of albedo and sea-ice feedback. Below a given threshold (situated between 2 and 3 PAL), the pCO$_2$ drop enables sea-ice growth over the Arctic and, to a lesser extent, the subsistence of snow on the ground during the cold season, which increases winter surface albedo (Figure 3). In addition, seasonal sea-ice expansion limits ocean-to-air heat transfer at highest Northern latitudes and contributes to further winter cooling of the atmosphere. This preferential lowering of winter temperatures results in a large MATR increase of 5-20% (3X-4X and 2X-3X) and up to 40% (2X-4X; Figure 4 e and S3 b) over high northern latitudes. Furthermore, the areas of colder winters and high MATR widen as pCO$_2$ decreases: MATR increases from 60°N poleward between 4X and 3X, to 50°N poleward between 4X and 2X (Figures 4 and S4). In contrast, Antarctica shows moderate ΔMATR (regionally up to 3°C from 4X to 3X, and 6°C from 3X to 2X) compared to high northern latitude lands (6°C MATR increase from 4X to 3X and 3X to 2X, and 10°C from 3X to 2X). This is because Antarctica is characterized by wide MATR values in all ice-sheet free experiments (4X, 3X and 2X experiments), resulting in low ΔMATR changes from one experiment to another (Figure 4 a,b). This important seasonality is induced by the continent's high albedo variability, as it oscillates from snow-free to snow-covered soil within a year.

3.1.3 Areas with decreased seasonality

Areas with decreased seasonality are characterized by summer cooling that exceeds winter cooling, which reduces the MATR (Figures 2 and 4). The widest zones of decreasing MATR are continental regions located within the 30-50° latitudinal band. The magnitude of simulated MATR reduction depends on the pCO$_2$ drop considered, with reduction from 3X to 2X and from 4X to 2X resulting in up to 20 and 30% of regional MATR decrease, respectively (Figures 4 and S3). At lower latitudes, in Amazonia, equatorial Africa and India, seasonality decreases but to a lesser extent (Figure 4). A variety of atmospheric and oceanic processes are likely involved in these contrasting MATR changes, depending on the region considered.

The good correlation between MATR increase (respectively decrease) and P-E ratio (i.e., precipitation *minus* evaporation, also referred to as *net precipitation*) decrease (respectively increase; i.e., North America, Central Asia, and North Australia) suggests a strong implication of the hydrological cycle on this phenomenon (Figures 5 and 6 a,c,h). The pCO$_2$ drop tends to

slow down the hydrological cycle, which results in flatter P-E latitudinal gradients. At high latitudes, a reduction of precipitation leads to an overall P-E decrease, while at mid to low latitudes, increased precipitation results in a general increase of P-E (Figures 5 and 6). In these low to mid latitude zones, precipitation strengthening is more important in summer and associated with increased evaporation, which results in larger latent heat fluxes and thus in a greater cooling during summer, consistently with decreased seasonality (Figure 6 a,c,h). In addition, summer cooling is strengthened through vegetation feedback: P-E increase favors net primary productivity which in turn contributes to evaporation and summer warmth loss (Figure 6 a,c,h). In contrast, decreased MATR in Europe and Southern South America appears poorly correlated to the above-mentioned parameters (Figure 6 b,g). For Europe, the presence of sea-ice over the Arctic Ocean (Figure 3 b-e) limits heat loss via the atmosphere during winter and results in a greater summer cooling of the SST (Figure S5), which contributes to lowering European MATR. In addition, a regional increase in low-level cloud cover during summer could also contribute to lowering ΔMATR for both Europe and southern South America through albedo feedback (5 to 15% higher low-level cloud fraction between 40-60°; Figure 7 and S6). For southern South America, several parameters seem consistent with the reduction of the MATR but it is difficult to disentangle their contribution. By amplifying the latitudinal temperature gradients, the pCO_2 drop induces a northward migration of the westerly wind maximum (by about 2° of latitude, annually but less markedly during austral winter, JAS) and of the Antarctic Circumpolar current, which delimits the southern hemisphere subpolar and subtropical gyres. This northward shift thereby limits the arrival of warm subtropical waters towards the poles (Figure S7). This greater cooling in summer SST reinforces the ocean's buffering effect on atmospheric temperatures in southern South America and favors milder summers, and to a lesser extent, cooler winters, which is consistent with a decrease in seasonality (Figures 4 and 7). Finally, changes in atmospheric dynamics (decrease in the width and increase in the intensity of the Hadley cell) are also visible and could have an impact on air-ocean exchanges, but much more analysis would be needed to understand their implication, which is not the focus of this paper (Figure S8).

3.2 Modelled response to Antarctic Ice Sheet and sea-level drop

3.2.1 Antarctic Ice Sheet only

AIS formation is responsible for a supplementary 0.9°C and 0.3°C cooling of the air temperature and the surface ocean respectively (Table 1). Its direct effect on 2 meter mean annual temperatures varies regionally and is more striking over Antarctica with up to -35°C cooling, and over the Southern Ocean and Australia (Figures 2 c,g,k and S3 c,d). In contrast with Arctic sea-ice which increases seasonality at highest northern latitudes, the AIS decreases southern latitude temperature seasonality (Figures 4 c and S3 c,d). Indeed, simulations with the AIS have a year-long white Antarctica with high and stable albedo, which reduces seasonal temperature variability (Figure 3 g-l).

3.2.2 Sea-level drop

Sea-level decrease alone is responsible for a 1.0°C cooling of global MAT (0.7°C for surface oceans) and results in considerable regional temperature changes in areas suffering important land-sea distribution changes (Table 1, Figures 4 d,f and S3 e,f). The marine regions that become exposed after sea level drop show the strongest increase in MATR, as they experience both winter cooling and summer warming, due to the lower thermal inertia of land compared to ocean. This seasonality strengthening in newly exposed areas occurs independently of their latitude, therefore disrupting the otherwise zonal distribution of seasonal temperature changes generated by pCO$_2$ drop and AIS formation (Figures 4 f and S3 f). The effect on seasonality of these disappearing seas expands beyond these areas adjoining the emerging landmasses due to the resulting regional perturbation in temperature. Northern Africa, Western Asia and Russia are the most impacted areas, due to the proto-Paratethys sea retreat and the emergence of the Arabian Peninsula (Figure 1). More moderate seasonality changes are also visible as a result of sea retreats of smaller extent, such as the emergence of the Florida platform and the modification of the East Asian coastlines (Figures 4 d and S3 e,f).

3.3 Model-data comparison

3.3.1 pCO$_2$ lowering

The ΔMATR described by the pCO$_2$ drop experiments (from 3X or 4X to 2X) show neither a good agreement with middle to late Eocene, nor with late Eocene to early Oligocene data estimates (Figures 4 a,b and 8 b). The simulations predict no change, or a MATR decrease, in areas where the Lutetian–Priabonian data points (n=6, triangles, Figure 4 a) describe increased seasonality (Figure 4 a,b). Priabonian–Rupelian ΔMATR modelled through 4X to 2X and 3X to 2X pCO$_2$ drops are, on average, lower than data estimates at similar localities, with a mean offset of -3.5 and -2.8°C, respectively (Figure 8 b; Table 2). The use of the simulation 4X instead of 3X for the late Eocene stage has a marginal effect on the percentage of agreement for the sign of the ΔMATR, although slightly higher value is observed for 3X-2X (Table 2, line '%', Figures 8 b and S9). In addition, pCO$_2$ drop alone leads to zonal ΔMATRs which do not transcribe the spatial heterogeneity visible in data. This misfit is visible through high RMSE scores and the absence of significant correlation between modelled ΔMATR resulting from pCO$_2$ drop (simulations 2X – 4X and 2X – 3X) and ΔMATR described by proxy-data (Table 2). Two data-model agreement patterns are nevertheless to be noted: (1) Regardless of their values (which are higher in data than in our simulations), the northernmost data points are inside or surround the high-latitude seasonality strengthening zone we modelled (Figure 4, data-points 1,2,3 on Figure 8 a); (2) none of the Southern Hemisphere data localities showing no seasonality change are located within MATR increase zones (Figure 4 b).

3.3.2 Antarctic ice-sheet and sea-level

The formation of the AIS alone does not result in a better agreement between modelled and Priabonian–Rupelian ΔMATR estimates. It is even slightly reduced (Table 2). The reinforcement of the MATR lowering zone at high-southern latitudes

increases the data-model misfit because of data points indicating null ΔMATR in this zone (Figure 4 c and Figure 8 b). There is still no significant correlation between ΔMATR from the model and differences documented by proxy-data (Table 2).

Geographic changes associated with sea-level drop result in a better agreement with data ΔMATR (Figure 4 d and 8 b). The largest continental fraction changes affect the MATR on a broad geographic scale and allow for a better agreement, even with several data points standing away from the regions directly impacted by the sea-level drop, as for example data estimates located on the Pacific Coast (Figure 4d). Similarly, coastline changes along the eastern part of Africa and Western Asia cause an increase in seasonality in Anatolia and Central/Western Europe, improving the fit between model and data. These changes in temperature seasonality result in a reduction of 2 to 2.5 months in the duration of the plant growing season (as reconstructed with the formula of Grein et al., 2013; Table S1). Smaller changes in coastlines such as in Florida, Kamchatka Peninsula or along the East Asian coast increase seasonality at a regional scale and improve the data-model fit (data-points 14, 22, 24). This better fit is transcribed through the RMSE analysis results, the lowest values being obtained when the simulation 2X-ICE-SL is used to simulate the Rupelian stage (Table 2). However, there is no significant correlation between model and proxy-data Priabonian–Rupelian ΔMATR, independently of the late Eocene simulation (4X or 3X) used as initial stage (for both, Spearman rank test: rho = 0.29, *p-value* = 0.12, Table 2). This persistent mismatch may be triggered by biases from the model or the data and from the methodology used to calculate these ΔMATR, which are further detailed in the Discussion. ΔMATR is still slightly underestimated by the model (Figure 8 b; Table 2). The pair of simulation that best describe the Priabonian-Rupelian transition, according to currently available data is 2X-ICE-SL – 3X as it presents (1) the lowest average model – data ΔMATR mismatch (-1.20°C) and (2) the best agreement in ΔMATR direction (45% of the data acerted, Table 2).

4 Discussion

4.1 Implication for mechanisms of late Eocene to early Oligocene seasonality changes

4.1.1 Model climate sensitivity and climate response to EOT forcing

ΔMATR across the EOT are better predicted when considering the changes occurring between the lower pCO_2 simulation 3X for the late Eocene stage and the most realistic simulation 2X-ICE-SL for the early Oligocene stage. In addition, with a mean SST cooling of 2.7°C between 3X and 2X simulations (Table 1), surface temperature changes are also in agreement with the mean changes described in marine proxies across the EOT (i.e., difference of 2.9°C between 38-34.2 and 33.7-30 Ma, Hutchinson et al., 2021). The best fit with a limited drop of pCO_2 reflects the high climate sensitivity of our model (i.e., the average temperature change per doubling of the pCO_2 at model equilibrium; PALEOSENS, 2012). This high sensitivity is also highlighted in our experiments of pCO_2 halving from 1120 to 560 ppm (2X-4X), which result in a dramatic mean annual global cooling (5.8°C for global MAT, 5°C for SST, Table 1). Such temperature difference is high compared to previous modelling studies which describe a 3 to 4°C surface atmospheric temperature difference under similar $pCO2$ decrease, and the 2.9°C cooling found in marine proxies across the EOT (Hutchinson et al., 2021). The pCO_2 of 4X and 2X, are more generally used

in simulations to represent the transition to an icehouse world (e.g., Baatsen et al., 2020; Goldner et al., 2014; Kennedy-Asser et al., 2019). Although 4X is likely to represent the upper end of pCO_2 possible values for the late Eocene (values rather approximate ~ 800 ppm from the Lutetian to the Priabonian; Foster et al., 2017), the use of this value is justified to better reconstruct high-latitudes temperatures (Huber and Caballero, 2011). A good agreement between warm conditions and Bartonian SST data has also been recently shown by other experiments using the model IPSL-CM5A2 with middle / late Eocene boundary conditions (Tardif et al., 2020; Toumoulin et al., 2020). We thus argue that the use of the 4X simulation is appropriate to study possible variations of pCO_2 during the Eocene, but the use of the 3X simulation is better to study the changes between the Priabonian and the Rupelian.

4.1.2 Temperature seasonality changes through the late Eocene

The evolution of the different climate features likely involved in ΔMATR is consistent with several findings from previous studies. First, earlier modelling experiments have described albedo and sea-ice increase resulting in polar amplification of the cooling (e.g., Baatsen et al., 2020; Kennedy-Asser et al., 2019) and a reinforcement of temperature seasonality (Eldrett et al., 2009). The resulting strengthening and expansion of the northern high-latitudes MATR increase zone with pCO_2 lowering is a good explanation for the dramatic seasonality increase at high latitudes suggested by some studies (Eldrett et al., 2009; Wolfe, 1992; Zanazzi et al., 2015). In addition, changes in the magnitude and distribution of net precipitation (i.e., precipitation – evaporation) resulting from the decrease in pCO_2 agree with former theoretical and modelling work suggesting an intensified hydrological cycle under higher pCO_2 (e.g., Carmichael et al., 2016; Hutchinson et al., 2018). This phenomenon results from a greater capacity of the air to retain moisture and more intense atmospheric convection phenomena (Allen and Ingram, 2003; Carmichael et al., 2016; Held and Soden, 2006). In parallel, although the implication of changes in the atmospheric circulation in the southern South American seasonality lowering zone appears non-obvious, the intensification and weakening of the Hadley cell extent in relation to changing pCO_2 levels have been described numerous times (e.g., Lu et al., 2007; Frierson et al., 2007). Deeper analyses would be needed to understand the atmospheric dynamics in the simulations, which is out of the scope of the study. Finally, the increase in low cloud cover is consistent with former model studies describing higher fraction of low-level clouds under lower pCO_2 (Baatsen et al., 2020; Caballero and Huber, 2013; Zhu et al., 2019). Nevertheless, although a low-level cloud cover increase due to pCO_2 drop is consistent with increased air moisture in Western Europe at the EOT (Kocsis et al., 2014), this parameter remains poorly constrained in paleoclimate archives and modelling analysis (Lunt et al., 2020; Sagoo et al., 2013).

Despite these agreements, the MATR evolution resulting from pCO_2 drop does not clearly match data estimates whether they correspond to both Lutetian-Priabonian or to Priabonian-Rupelian changes. This suggests that the temperature seasonality inferred from proxy data can only be partly explained by a pCO_2 drop. Since zonal ΔMATR patterns are simulated with a pCO_2 drop of 1PAL (either from 4X to 3X or from 3X to 2X) we hypothesize that they likely occurred before the AIS onset, and that the strengthening of seasonality occurred in northern high-latitudes in the first place. However, most of Lutetian-Priabonian data are not located in the high-latitudes, which prevents unambiguous testing of this hypothesis (Figure 4 a,b and

Table S1). Similarly, the presence of areas with decreased seasonality due to changes in the hydrological cycle (i.e., USA, Central Asia, north Australia) cannot be confirmed because of a lack of data in these areas: although some of the data associated with a decrease in the MATR share the same latitudinal bands, none of them are directly located within a zone of MATR decrease. New additional seasonal temperature records in these areas would be interesting to better trace such eventual early trends. The general low fit of data and model values for middle to late Eocene changes is, to some extent, predictable since the ice-free 2X simulation does not represent the late Eocene (see Material and Method section) and was designed as a sensitivity test. Indeed, small scale glaciations (25-35% modern AIS) may have existed during the late Eocene, before the EOT, associated with a moderate sea-level decrease (Carter et al., 2017; Miller et al., 2020; Scher et al., 2014). Interestingly, the combination of the three forcing mechanisms leads to a better agreement of the modelled ΔMATR with middle to late Eocene data, especially in coastal areas of Kamchatka, and South China (triangles, Figure 4). Although the 70-m sea level decrease prescribed in the 2X-ICE-SL simulation is unrealistic for the late Eocene, the better data-model agreement when both AIS and sea-level decrease are considered suggests that small ice-sheet development before the EOT may have played a significant role in driving the middle to late Eocene ΔMATR. Additional sensitivity experiments, with a smaller AIS and an intermediated sea-level drop, may allow further quantification of the sensitivity of coastal localities to sea-level variations occurring before the EOT.

4.1.3 Temperature seasonality changes through the EOT

The use of two simulations to set up the effect of the AIS onset (with or without a drop-in sea level) is interesting to unravel the direct and indirect mechanisms affecting temperatures. Temperature changes resulting from the presence of the AIS alone (i.e., not taking into account sea level) are consistent with former model studies that simulate a highly regional effect on atmospheric temperature (see supporting information of Hutchinson et al., 2021), although the changes in our simulations spread more widely over the Southern Ocean and Australia. The decreasing seasonality zones modelled at high and mid-latitudes of the Southern Hemisphere are mostly associated with an absence of seasonality change in the data, which often display stable vegetation and biomes from the late Eocene to the Rupelian (Hutchinson et al., 2021; Kohn et al., 2015; Nott and Owen, 1992; Pocknall, 1989; Pound and Salzmann, 2017). This apparent mismatch calls into question the capability of paleobotanical proxies to record temperature seasonality decrease in environments already characterized by low seasonality. Indeed, the decrease in the temperature seasonality is associated with a more pronounced drop in summer temperatures, which is a less limiting factor for flora distribution and thus less constrained in the fossil record than winter temperatures (Huber and Caballero, 2011).

The evolution of temperature seasonality from the Priabonian to the Rupelian is better represented when the sea level drop associated with the AIS is taken into account (Table 2, Figures 4 and 8). This consequence of the Antarctic glaciation has global repercussions and explains part of the heterogeneity documented in the data, as previously suggested (Pound and Salzmann, 2017). Our results are very dependent on the paleogeography used in the simulations and of the proxy location used in our data-model comparison. Because our Rupelian simulations use a late Eocene paleogeography with a global sea level

decrease, we overlook some paleogeographic changes that occurred between both periods, which may affect our seasonality reconstruction. The gradual northward migration of Australia is not considered; the Neotethys is gradually closed during the early Oligocene but a deep-sea passage to the north of the Arabian Plate remains present in our paleogeography (Barrier et al., 2018). Another source of error may come from fragmented continental areas such as those seen in Europe at that time. In these zones, temperature changes recorded through the EOT are heterogeneous as paleovegetation studies suggest medium (1.8 - 2.1°C; Moraweck et al., 2019; Teodoridis et Kvaček, 2015; Tosal et al., 2019) to strong (up to 8.3°C; Tanrattana et al., 2020) MATR increase. The heterogeneity shown in data might thus result from smaller scale paleogeographic changes through the EOT that are not well represented by the resolution used in our simulations. This variability of data ΔMATR estimate could also be due to (1) a variable quality of MATR data related to the fragmentary nature of the fossil record and to differential recording of vegetation types, as well as (2) differences in the temperature of marine/oceanic zones before regression. Depending on their extension and depth, these seas may have buffered more or less importantly seasonal temperature variations of the nearby regions, and therefore their disappearance may have affected the MATR in different magnitudes. An early Oligocene intensification of seasonality in Central and Eastern Europe, associated to major phase of Antarctic ice-sheet expansion (and its effect on sea level), is consistent with fairly stable vegetation between the middle and late Eocene (Bozukov et al., 2009; Kvaček et al., 2014; Moraweck et al., 2015). This may result from the proximity with the warm Tethys, buffering the EOT cooling, as suggested by stable δ^{18}O describing moderate temperature changes in this area (Kocsis et al., 2014).

Finally, differences between our modelling results and data may also be related to the amplitude of the sea-level drop used in our simulation compared to its variability during the Rupelian. The EOT is generally described in two steps: a first event at ~ 33.9 Ma with both a decrease in temperature and sea level (~ 25 m) and a second event, the Early Oligocene Glacial Maximum (EOGM), between approximately 33.65 and 33.15 Ma, starting after a large oxygen isotope incursion (often referred to as "Oi-1"), which is characterized by an additional 50 m sea-level decrease (see Hutchinson et al., 2021 for synthesis and terminology, and Miller et al., 2020). The sum of these two steps corresponds to the boundary conditions of our simulation. However, important variations of the East Antarctic Ice-Sheet have been described until the early Miocene (50-60 m sea-level equivalent; Miller et al., 2020). Directly after the EOGM phase, a decrease in ice-volume is visible between 33.15 and 32.8 Ma, before increasing again and remaining stable between 32.8 and 29 Ma (after the "Oi-1a" event; Galeotti et al., 2016). Due to the combined effects of the drop in CO_2 and the development of the AIS (and the amplitude of the associated drop in sea level, 70 m), the important changes in seasonality reconstructed here (2X-ICE-SL *minus* 3X) were probably not in place throughout the Rupelian, but rather for shorter periods during the EOGM, or later between 32.8-29 Ma. Most continental paleoclimate studies do not provide the resolution to distinguish these steps. Among the data points compiled for this study, only four sites have enough temporal resolution to be linked to the EOGM phase represented by our 2X-ICE-SL simulation (Bozukov et al., 2009; Eldrett et al., 2009; Hren et al., 2013; Kohn et al., 2015; Tosal et al., 2019).

4.2 Perspectives on environmental and biotic crisis

The EOT is associated with major extinction events, of which the best known are the "Grande Coupure" in Europe and the "Mongolian Remodelling" in central Asia (Stehlin, 1909; Meng and McKenna, 1998; see Coxall and Pearson, 2007 for review). Both events were recognized as major biotic turnovers for ungulates (Blondel, 2001; Stehlin, 1909). In addition, other vertebrates were affected by the Grande Coupure (e.g., rodents, primates, amphibians and squamates), and major changes in vegetation are described, in association to the Mongolian Remodelling, and regionally, in Europe (e.g., Barbolini et al., 2020; Dolezych et al. in press; Eldrett et al., 2009; Marigó et al., 2014; Pound and Salzmann, 2017; Rage, 1986, 2013; Rage and Roček, 2003). These changes have been linked to (1) competitive interactions resulting from the dispersal of Asian taxa to Europe, and (2) EOT climate deterioration and selection processes through resource and/or habitat changes (e.g. Hooker et al., 2004; Kratz and Geisler, 2010; Marigó et al., 2014; Sun et al., 2015; Zhang et al., 2012). The latter mechanism is commonly related to irreversible cooling and/or aridification at the EOT (e.g., Blondel, 2001; Sun et al., 2015; Zhang et al., 2012). Climate cooling may have significantly reduced the habitat of well spread early Eocene tropical (and paratropical) species, which are characterized by narrow thermal ecological niches (Hren et al., 2009; Huang et al., 2020; Jaramillo et al., 2006; Wing, 1987). Although the distribution of fauna and flora is based on a complex set of parameters, we discuss here how ΔMATR provides an additional interpretative key for understanding biotic turnover at the EOT.

While North America and Asia show comparable temperature changes, our simulations highlight significant differences in the evolution of their MATR, which decrease and either increase/decrease at a regional scale, respectively. Vegetation changes and the Mongolian Remodelling are contemporaneous to AIS growth between 32.8-29 Ma and can be compared with our 2X-ICE-SL simulation (Galeotti et al., 2016; Kraatz and Geisler, 2010; Sun et al., 2015). The MATR strengthening modelled in central Asia shows that cooling was particularly strong during winter. In addition to the aridification, this more pronounced winter-cooling may have contributed to the intensity of extinctions in this area (Barbolini et al., 2020; Dupont-Nivet et al., 2007). This seasonality strengthening is strongly driven by the proto-Parathethys retreat, which contrasts with a previous geochemistry study suggesting a weak contribution of this sea to local climate conditions (Bougeois et al., 2018). Conversely, the zone of decreased MATR reconstructed in North America may provide an explanation for the low impact of the EOT on fauna and vegetation in this area (Coxall and Pearson, 2007; Prothero and Heaton, 1996; Stucky, 1992). Despite a similar decrease of the mean annual temperature, most of the temperature drop is in summer and is not associated with the onset of cold winters (Figure S4). We hypothesize that these patterns enabled a greater persistence of existing warm-temperate to paratropical vegetation and associated biota (Pound and Salzmann, 2017). The study of Tardif et al. (2021) using the same model and similar simulations (4X and 2X-ICE) with a dynamic vegetation module shows moderate biome changes across the EOT in this North America decreased seasonality zone. Reduced stress on biodiversity in areas with limited or reduced MATR changes is also consistent with moderate vegetation changes across the EOT in areas with decreasing seasonality in the Southern Hemisphere (see discussion 4.1.3).

Europe stands in an intermediate position between North America and Asia with generally weaker changes in MATR (Figure 4 d); Eastern Europe exhibits a slight increase in MATR, while MATR decreases in the west. Although comparable ΔMATR values could have different impacts depending on initial MATR, the types of ecosystems and their resilience, the strong
475 consequences of moderate seasonality increase on growing season length supports the hypothesis that seasonality changes may also have contributed to shaping the biodiversity evolution in Central Europe. The late development of increased seasonality zones in this area, linked to the major phase of sea level drop, could explain the persistence of fairly stable vegetation during the Eocene (Kvaček et al., 2014; Hutchinson et al., 2021). Yet, given the fragmented nature of Europe at this time, increases in seasonality prior to EOT would also be possible as a result of smaller, but locally significant, sea level variations. These
480 differences in the evolution of the MATR between North America, Europe and Asia support several studies suggesting different causes for EOT extinctions (Blondel, 2001; Hooker et al., 2004; Meng and McKenna 1998; Sun et al., 2015). Finally, little is known about the EOT in Africa (notably because of a few Oligocene sites), but the data available suggest moderate changes in northern African flora and fauna (Hutchinson et al., 2021; Jacobs et al., 2010; Pound and Salzmann, 2017; Rasmussen et al., 1992). The significant increase in seasonality in North Africa seen in our simulations (which results from
485 the emergence of part of the continent), differs from the one observed in other areas, since it is linked to an increase in summer temperatures (barely no change in winter). Unchanged winter temperatures and shift of marine to terrestrial environments might complicate the recording of this temperature seasonality strengthening. Recording low latitude changes in seasonality strengthening may however be possible as shown by a recent study combining multiple lines of evidences (including plant and primate macrofossils), which suggest a potential shift from tropical to more open deciduous vegetation through the EOT,
490 reflecting increased seasonality in precipitation and/or temperature seasonality during the early Oligocene at low latitudes of South America (Peru, ~7°S, Antoine et al., 2021). More studies would probably enable a better understanding of the evolution of the seasonality in this low latitude area.

5 Conclusion

This study investigates the changes in temperature seasonality during the middle to late Eocene and across the EOT. MATR
495 changes modelled with the combined effects of pCO_2 drop, AIS formation and sea-level lowering are qualitatively consistent with the proxy data reconstruction of the late Eocene to early Oligocene. The decrease in pCO_2 leads to a marked strengthening of seasonality in the northern high-latitudes, which may have started earlier than the EOT, during the late Eocene. The formation of the AIS and the resulting sea-level drop lead to both an intensification and an extension of increasing seasonality areas. The best agreement between data and modelled MATR evolution throughout the EOT is reached when all three
500 parameters are combined. Accounting for sea level changes associated with the Antarctic glaciation appears to be the most important parameter to explain the heterogeneity of ΔMATR across the EOT. A seasonality increase is also visible in middle to late Eocene localities, which may reflect earlier sea level changes associated with the incipient precursors of the Antarctic ice sheet. A discrepancy between data and model is present for quantitative MATR change estimates across the EOT, with less marked seasonality changes in the model. This is mainly due to areas where a decrease in seasonality is predicted by the model

505 while the vegetation proxies show stable vegetation. We hypothesize that this discrepancy can be explained by a low capacity of vegetation to record decreases in summer temperatures compared to winter temperatures.

Reconstructing changes in MATR brings additional constraints on the abiotic environmental factors at play on land between the middle Eocene and the early Oligocene. The different mechanisms described here likely explain the heterogeneity in seasonality changes found in data across the greenhouse-icehouse transition, and provide insights into the diversity of

510 continental paleoenvironments. The map of ΔMATR reconstructed here may provide new elements to better understand major extinction events at the EOT. This study primarily focused on the evolution of temperature seasonality that has the clearest evolution. The variability of other seasonality parameters, including rainfall seasonality, will be worth investigating in future studies to obtain a finer picture of the evolution of terrestrial climates and biodiversity through the EOT. In addition, further work using higher resolution Rupelian paleogeography and regional models would be of great interest to better reconstruct

515 temperature seasonality changes, especially in highly fragmented land areas such as Europe during the Eocene.

Code availability

LMDZ, XIOS, NEMO and ORCHIDEE are released under the terms of the CeCILL license. OASISMCT is released under the terms of the Lesser GNU General Public License (LGPL). IPSL-CM5A2 code is publicly available through svn, with the following command lines: svn co

520 http://forge.ipsl.jussieu.fr/igcmg/svn/modipsl/branches/publications/IPSLCM5A2.1_11192019 (last access: 16 February 2021, IPSL Climate Modelling Centre, 2021a) modipsl cd modipsl/util;./model IPSLCM5A2.1

The mod.def file provides information regarding the different revisions used, namely

- NEMOGCMbranchnemo_v3_6_STABLErevision666-XIOS2branchs/xios-2.5revision1763
- IOIPSL/srcsvntags/v2_2_2
525 - LMDZ5branches/IPSLCM5A2.1rev3591
- branches/publications/ORCHIDEE_IPSLCM5A2.1.r5307rev6336–OASIS3-MCT2.0_branch(rev4775IPSLserver)

The login/password combination requested for the first use to download the ORCHIDEE component is anonymous/anonymous. We recommend referring to the project website http://forge.ipsl.jussieu.fr/igcmg_doc/wiki/Doc/Config/IPSLCM5A2 (last access: 16 February 2021, IPSL Climate Modelling

530 Centre, 2021b) for a proper installation and compilation of the environment.

Data availability

The key climatological outputs of the simulations are stored in the PANGAEA database: https://doi.pangaea.de/10.1594/PANGAEA.930422

Author contribution

YD, AT and JBL conducted the modelling experiments. AT compiled proxy-data, analysed the model results, generated Figures and tables, and drafted the manuscript. AT, YD, DT and JBL discussed the paleoclimate results. LK contributed to the paleobotanical context, and AL and GDN to the paleogeographic and geological context. All authors have provided critical feedback and contributed to the final manuscript.

Competing interests

The authors declare that they have no conflict of interest.

Acknowledgment

We thank the CEA/CCRT for providing access to the HPC resources of TGCC under the allocation 2018-A0030102212, and 2019-A0050102212 made by GENCI. AT and GDN acknowledge the support of the ERC MAGIC under Grant 649081. The authors acknowledge Cheng-Sen Li for sharing a translation of the reference Budantsev (1997). We acknowledge the use of Ferret (ferret.pmel.noaa.gov/Ferret/) and RStudio software (rstudio.com) for analysis and Figures in this paper. We sincerely thank Alberto Reyes for his editorial handling and two anonymous reviewers for their interesting comments that improved the quality of this article.

References

Abbot, D. S., and Tziperman, E. (2008). A high-latitude convective cloud feedback and equable climates. Quarterly Journal of the Royal Meteorological Society, 134(630), 165–185. https://doi.org/10.1002/qj.211

Allen, M. R., and Ingram, W. J. (2002). Constraints on future changes in climate and the hydrologic cycle. Nature, 419(6903), 228–232. https://doi.org/10.1038/nature01092

Antoine, P.-O., Yans, J., Castillo, A. A., Stutz, N., Abello, M. A., Adnet, S., Custódio, M. A., Benites-Palomino, A., Billet, G., Boivin, M., Herrera, F., Jaramillo, C., Mártinez, C., Moreno, F., Navarrete, R. E., Negri, F. R., Parra, F., Pujos, F., Rage, J.-C., … Marivaux, L. (2021). Biotic community and landscape changes around the Eocene–Oligocene transition at Shapaja, Peruvian Amazonia: Regional or global drivers? Global and Planetary Change, 202, 103512. https://doi.org/10.1016/j.gloplacha.2021.103512

Aumont, O., Ethé, C., Tagliabue, A., Bopp, L., and Gehlen, M. (2015). PISCES-v2: An ocean biogeochemical model for carbon and ecosystem studies. Geoscientific Model Development, 8(8), 2465–2513. https://doi.org/10.5194/gmd-8-2465-2015

Baatsen, M., von der Heydt, A. S., Huber, M., Kliphuis, M. A., Bijl, P. K., Sluijs, A., and Dijkstra, H. A. (2020). The middle to late Eocene greenhouse climate modelled using the CESM 1.0.5. Climate of the Past, 16(6), 2573–2597. https://doi.org/10.5194/cp-16-2573-2020

565   Barbolini, N., Woutersen, A., Dupont-Nivet, G., Silvestro, D., Tardif, D., Coster, P. M. C., Meijer, N., Chang, C., Zhang, H.-X., Licht, A., Rydin, C., Koutsodendris, A., Han, F., Rohrmann, A., Liu, X.-J., Zhang, Y., Donnadieu, Y., Fluteau, F., Ladant, J.-B., … Hoorn, C. (2020). Cenozoic evolution of the steppe-desert biome in Central Asia. Science Advances, 6(41), eabb8227. https://doi.org/10.1126/sciadv.abb8227

Barrier, E., Vrielynck, B., Brouillet, J.-F., and Brunet, M.-F. (2018). Paleotectonic Reconstruction of the Central Tethyan Realm. Tectonono-Sedimentary-Palinspastic maps from Late Permian to Pliocene. CCGM/CGMW, Paris, 570   http://www.ccgm.org.

Bishop, P., and Bamber, R. K. (1985). Silicified wood of Early Miocene Nothofagus, Acacia and Myrtaceae (aff. Eucalyptus B) from the upper Lachlan valley, New South Wales. Alcheringa: An Australasian Journal of Palaeontology, 9(3), 221–228. https://doi.org/10.1080/03115518508618969

Blondel, C. (2001). The Eocene–Oligocene ungulates from Western Europe and their environment. Palaeogeography, 575   Palaeoclimatology, Palaeoecology, 168(1), 125–139. https://doi.org/10.1016/S0031-0182(00)00252-2

Bougeois, L., Dupont-Nivet, G., de Rafélis, M., Tindall, J. C., Proust, J.-N., Reichart, G.-J., de Nooijer, L. J., Guo, Z., & Ormukov, C. (2018). Asian monsoons and aridification response to Paleogene sea retreat and Neogene westerly shielding indicated by seasonality in Paratethys oysters. *Earth and Planetary Science Letters*, *485*, 99–110. https://doi.org/10.1016/j.epsl.2017.12.036

580   Bozukov, V., Utescher, T., and Ivanov, D. (2009). Late Eocene to early Miocene climate and vegetation of Bulgaria. Review of Palaeobotany and Palynology, 153(3–4), 360–374. https://doi.org/10.1016/j.revpalbo.2008.10.005

Budantsev, L.Y., 1997. Late Eocene flora of western Kamchatka. Proceedings of Komarov Botanical Institute, Russian Academy of Sciences. 19, pp. 1–115 (in Russian).

Caballero, R., and Huber, M. (2013). State-dependent climate sensitivity in past warm climates and its implications for future 585   climate projections. Proceedings of the National Academy of Sciences, 110(35), 14162–14167. https://doi.org/10.1073/pnas.1303365110

Carmichael, M. J., Lunt, D. J., Huber, M., Heinemann, M., Kiehl, J., LeGrande, A., Loptson, C. A., Roberts, C. D., Sagoo, N., Shields, C., Valdes, P. J., Winguth, A., Winguth, C., and Pancost, R. D. (2016). A model–model and data–model comparison for the early Eocene hydrological cycle. Climate of the Past, 12(2), 455–481. https://doi.org/10.5194/cp-12-455-2016

590   Carter, A., Riley, T. R., Hillenbrand, C.-D., and Rittner, M. (2017). Widespread Antarctic glaciation during the Late Eocene. *Earth and Planetary Science Letters*, 458, 49–57. https://doi.org/10.1016/j.epsl.2016.10.045

Colwyn, D. A., & Hren, M. T. (2019). An abrupt decrease in Southern Hemisphere terrestrial temperature during the Eocene–Oligocene transition. *Earth and Planetary Science Letters*, 512, 227–235. https://doi.org/10.1016/j.epsl.2019.01.052

Coxall, H. K., and Pearson, P. N. (2007). The Eocene–Oligocene Transition. In M. Williams, A. M. Haywood, F. J. Gregory, 595   and D. N. Schmidt (Eds.), Deep-Time Perspectives on Climate Change: Marrying the Signal from Computer Models and Biological Proxies (First, pp. 351–387). The Geological Society of London on behalf of The Micropalaeontological Society. https://doi.org/10.1144/TMS002.16

Coxall, H. K., Wilson, P. A., Pälike, H., Lear, C. H., and Backman, J. (2005). Rapid stepwise onset of Antarctic glaciation and deeper calcite compensation in the Pacific Ocean. Nature, 433(7021), 53–57. https://doi.org/10.1038/nature03135

600   Dufresne, J.-L., Foujols, M.-A., Denvil, S., Caubel, A., Marti, O., Aumont, O., Balkanski, Y., Bekki, S., Bellenger, H., Benshila, R., Bony, S., Bopp, L., Braconnot, P., Brockmann, P., Cadule, P., Cheruy, F., Codron, F., Cozic, A., Cugnet, D., …

Vuichard, N. (2013). Climate change projections using the IPSL-CM5 Earth System Model: From CMIP3 to CMIP5. Climate Dynamics, 40(9–10), 2123–2165. https://doi.org/10.1007/s00382-012-1636-1

605 Dupont-Nivet, G., Krijgsman, W., Langereis, C. G., Abels, H. A., Dai, S., and Fang, X. (2007). Tibetan plateau aridification linked to global cooling at the Eocene–Oligocene transition. Nature, 445(7128), 635–638. https://doi.org/10.1038/nature05516

Eldrett, J. S., Greenwood, D. R., Harding, I. C., and Huber, M. (2009). Increased seasonality through the Eocene to Oligocene transition in northern high latitudes. Nature, 459(7249), 969. https://doi.org/10.1038/nature08069

Fichefet, T., and Maqueda, M. A. M. (1997). Sensitivity of a global sea ice model to the treatment of ice thermodynamics and dynamics. Journal of Geophysical Research: Oceans, 102(C6), 12609–12646. https://doi.org/10.1029/97JC00480

610 Foster, G. L., Royer, D. L., and Lunt, D. J. (2017). Future climate forcing potentially without precedent in the last 420 million years. Nature Communications, 8(1), 14845. https://doi.org/10.1038/ncomms14845

Galeotti, S., DeConto, R., Naish, T., Stocchi, P., Florindo, F., Pagani, M., Barrett, P., Bohaty, S. M., Lanci, L., Pollard, D., Sandroni, S., Talarico, F. M., and Zachos, J. C. (2016). Antarctic Ice Sheet variability across the Eocene-Oligocene boundary climate transition. Science, 352(6281), 76–80. https://doi.org/10.1126/science.aab0669

615 Goldner, A., Herold, N., and Huber, M. (2014). Antarctic glaciation caused ocean circulation changes at the Eocene–Oligocene transition. Nature, 511(7511), 574–577. https://doi.org/10.1038/nature13597

Goldner, A., Huber, M., and Caballero, R. (2013). Does Antarctic glaciation cool the world? Climate of the Past, 9(1), 173–189. https://doi.org/10.5194/cp-9-173-2013

Gough, D. O. (1981). Solar interior structure and luminosity variations. Solar Physics, 74(1), 21–34.
620 https://doi.org/10.1007/BF00151270

Grein, M., Oehm, C., Konrad, W., Utescher, T., Kunzmann, L., and Roth-Nebelsick, A. (2013). Atmospheric CO2 from the late Oligocene to early Miocene based on photosynthesis data and fossil leaf characteristics. *Palaeogeography, Palaeoclimatology, Palaeoecology*, *374*, 41–51. https://doi.org/10.1016/j.palaeo.2012.12.025

Grimes, S. T., Hooker, J. J., Collinson, M. E., and Mattey, D. P. (2005). Summer temperatures of late Eocene to early Oligocene
625 freshwaters. Geology, 33(3), 189–192. https://doi.org/10.1130/G21019.1

Grimm, G. W., and Potts, A. J. (2016). Fallacies and fantasies: The theoretical underpinnings of the Coexistence Approach for palaeoclimate reconstruction. Climate of the Past, 12(3), 611–622. https://doi.org/10.5194/cp-12-611-2016

Held, I. M., and Soden, B. J. (2006). Robust Responses of the Hydrological Cycle to Global Warming. Journal of Climate, 19(21), 5686–5699. https://doi.org/10.1175/JCLI3990.1

630 Hooker, J. J., Collinson, M. E., and Sille, N. P. (2004). Eocene–Oligocene mammalian faunal turnover in the Hampshire Basin, UK: Calibration to the global time scale and the major cooling event. Journal of the Geological Society, 161(2), 161–172. https://doi.org/10.1144/0016-764903-091

Hourdin, F., Grandpeix, J.-Y., Rio, C., Bony, S., Jam, A., Cheruy, F., Rochetin, N., Fairhead, L., Idelkadi, A., Musat, I., Dufresne, J.-L., Lahellec, A., Lefebvre, M.-P., and Roehrig, R. (2013). LMDZ5B: The atmospheric component of the IPSL
635 climate model with revisited parameterizations for clouds and convection. Climate Dynamics, 40(9–10), 2193–2222. https://doi.org/10.1007/s00382-012-1343-y

Hren, M. T., Sheldon, N. D., Grimes, S. T., Collinson, M. E., Hooker, J. J., Bugler, M., and Lohmann, K. C. (2013). Terrestrial cooling in Northern Europe during the Eocene–Oligocene transition. Proceedings of the National Academy of Sciences, 110(19), 7562–7567. https://doi.org/10.1073/pnas.1210930110

640 Huang, H., Morley, R., Licht, A., Dupont-Nivet, G., Grímsson, F., Zetter, R., Westerweel, J., Win, Z., Wa Aung, D., and Hoorn, C. (2020). Eocene palms from central Myanmar in a South-East Asian and global perspective: Evidence from the palynological record. Botanical Journal of the Linnean Society. https://doi.org/10.1093/botlinnean/boaa038

Huber, M., and Caballero, R. (2011). The early Eocene equable climate problem revisited. Climate of the Past, 7(2), 603–633. https://doi.org/10.5194/cp-7-603-2011

645 Hutchinson, D. K., Coxall, H. K., Lunt, D. J., Steinthorsdottir, M., de Boer, A. M., Baatsen, M., von der Heydt, A., Huber, M., Kennedy-Asser, A. T., Kunzmann, L., Ladant, J.-B., Lear, C. H., Moraweck, K., Pearson, P. N., Piga, E., Pound, M. J., Salzmann, U., Scher, H. D., Sijp, W. P., … Zhang, Z. (2021). The Eocene–Oligocene transition: A review of marine and terrestrial proxy data, models and model–data comparisons. *Climate of the Past*, *17*(1), 269–315. https://doi.org/10.5194/cp-17-269-2021

650 Hutchinson, D. K., Coxall, H. K., O′Regan, M., Nilsson, J., Caballero, R., and de Boer, A. M. (2019). Arctic closure as a trigger for Atlantic overturning at the Eocene-Oligocene Transition. Nature Communications, 10(1), 3797. https://doi.org/10.1038/s41467-019-11828-z

Hutchinson, D. K., de Boer, A. M., Coxall, H. K., Caballero, R., Nilsson, J., and Baatsen, M. (2018). Climate sensitivity and meridional overturning circulation in the late Eocene using GFDL CM2.1. Climate of the Past, 14(6), 789–810.
655 https://doi.org/10.5194/cp-14-789-2018

IPSL Climate Modeling Centre: IPSL-CM5A-VLR branche IPSLCM5A2.1_11192019, available at: http://forge.ipsl.jussieu.fr/igcmg/svn/modipsl/branches/publications/IPSLCM5A2.1_11192019, last access: 16 February 2021a.

IPSL Climate Modeling Centre: IPSL climate models documentation, available at:
660 http://forge.ipsl.jussieu.fr/igcmg_doc/wiki/Doc/Config/IPSLCM5A2, last access: 16 February 2021b.

Ivany, L. C., Patterson, W. P., and Lohmann, K. C. (2000). Cooler winters as a possible cause of mass extinctions at the Eocene/Oligocene boundary. Nature, 407(6806), 887–890. https://doi.org/10.1038/35038044

Jacobs, B. F., Pan, A. D., and Scotese, C. R. (2010). A review of the Cenozoic vegetation history of Africa, in: Cenozoic mammals of Africa, edited by: Werdelin, W. J., Sanders, L., University of California Press, Berkeley, CA, 57–72.

665 Jaramillo, C., Rueda, M. J., and Mora, G. (2006). Cenozoic Plant Diversity in the Neotropics. Science, 311(5769), 1893–1896. https://doi.org/10.1126/science.1121380

Joomun, S. C., Hooker, J. J., and Collinson, M. E. (2010). Changes in dental wear of Plagiolophus minor (Mammalia: Perissodactyla) across the Eocene–Oligocene transition. Journal of Vertebrate Paleontology, 30(2), 563–576. https://doi.org/10.1080/02724631003618124

670 Katz, M. E., Miller, K. G., Wright, J. D., Wade, B. S., Browning, J. V., Cramer, B. S., and Rosenthal, Y. (2008). Stepwise transition from the Eocene greenhouse to the Oligocene icehouse. Nature Geoscience, 1(5), 329–334. https://doi.org/10.1038/ngeo179

Kayseri-Özer, M. S. (2013). Spatial distribution of climatic conditions from the Middle Eocene to Late Miocene based on palynoflora in Central, Eastern and Western Anatolia. Geodinamica Acta, 26(1–2), 122–157. https://doi.org/10.1080/09853111.2013.877237

Kennedy, A. T., Farnsworth, A., Lunt, D. J., Lear, C. H., and Markwick, P. J. (2015). Atmospheric and oceanic impacts of Antarctic glaciation across the Eocene–Oligocene transition. Philosophical Transactions of the Royal Society A: Mathematical, Physical and Engineering Sciences, 373(2054), 20140419. https://doi.org/10.1098/rsta.2014.0419

Kennedy-Asser, A. T., Lunt, D. J., Farnsworth, A., and Valdes, P. J. (2019). Assessing Mechanisms and Uncertainty in Modeled Climatic Change at the Eocene-Oligocene Transition. Paleoceanography and Paleoclimatology, 34(1), 16–34. https://doi.org/10.1029/2018PA003380

Kennedy-Asser, Alan T., Lunt, D. J., Valdes, P. J., Ladant, J.-B., Frieling, J., and Lauretano, V. (2020). Changes in the high-latitude Southern Hemisphere through the Eocene–Oligocene transition: A model–data comparison. Climate of the Past, 16(2), 555–573. https://doi.org/10.5194/cp-16-555-2020

Kocsis, L., Ozsvárt, P., Becker, D., Ziegler, R., Scherler, L., and Codrea, V. (2014). Orogeny forced terrestrial climate variation during the late Eocene–early Oligocene in Europe. Geology, 42(8), 727–730. https://doi.org/10.1130/G35673.1

Kohn, M. J., Strömberg, C. A. E., Madden, R. H., Dunn, R. E., Evans, S., Palacios, A., and Carlini, A. A. (2015). Quasi-static Eocene–Oligocene climate in Patagonia promotes slow faunal evolution and mid-Cenozoic global cooling. Palaeogeography, Palaeoclimatology, Palaeoecology, 435, 24–37. https://doi.org/10.1016/j.palaeo.2015.05.028

Kraatz, B. P., and Geisler, J. H. (2010). Eocene–Oligocene transition in Central Asia and its effects on mammalian evolution. Geology, 38(2), 111–114. https://doi.org/10.1130/G30619.1

Krinner, G., Viovy, N., de Noblet-Ducoudré, N., Ogée, J., Polcher, J., Friedlingstein, P., Ciais, P., Sitch, S., and Prentice, I. C. (2005). A dynamic global vegetation model for studies of the coupled atmosphere-biosphere system. Global Biogeochemical Cycles, 19(1). https://doi.org/10.1029/2003GB002199

Kunzmann, L., Kvacek, Z., Teodoridis, V., Müller, C., and Moraweck, K. (2016). Vegetation dynamics of riparian forest in central Europe during the late Eocene. Palaeontographica Abteilung B, 295, 69–89. https://doi.org/10.1127/palb/295/2016/69

Kvaček, Z. (2010). Forest flora and vegetation of the European early Palaeogene – a review. Bulletin of Geosciences, 85(1), 63–76. https://doi.org/10.3140/bull.geosci.1146

Kvaček, Z., Teodoridis, V., Mach, K., Přikryl, T., and Dvořák, Z. (2014). Tracing the Eocene-Oligocene transition: A case study from North Bohemia. Bulletin of Geosciences, 89(1), 21–66. https://doi.org/10.3140/bull.geosci.1411

Ladant, J.-B., Donnadieu, Y., and Dumas, C. (2014a). Links between CO2, glaciation and water flow: Reconciling the Cenozoic history of the Antarctic Circumpolar Current. Climate of the Past, 10(6), 1957–1966. https://doi.org/10.5194/cp-10-1957-2014

Ladant, J.-B., Donnadieu, Y., Lefebvre, V., and Dumas, C. (2014b). The respective role of atmospheric carbon dioxide and orbital parameters on ice sheet evolution at the Eocene-Oligocene transition: Ice sheet evolution at the EOT. Paleoceanography, 29(8), 810–823. https://doi.org/10.1002/2013PA002593

Lauretano, V., Kennedy-Asser, A. T., Korasidis, V. A., Wallace, M. W., Valdes, P. J., Lunt, D. J., Pancost, R. D., & Naafs, B. D. A. (2021). Eocene to Oligocene terrestrial Southern Hemisphere cooling caused by declining pCO2. *Nature Geoscience*, *14*(9), 659–664. https://doi.org/10.1038/s41561-021-00788-z

710 Lear, C. H., Bailey, T. R., Pearson, P. N., Coxall, H. K., and Rosenthal, Y. (2008). Cooling and ice growth across the Eocene-Oligocene transition. Geology, 36(3), 251. https://doi.org/10.1130/G24584A.1

Li, S., Xing, Y., Valdes, P. J., Huang, Y., Su, T., Farnsworth, A., Lunt, D. J., Tang, H., Kennedy, A. T., and Zhou, Z. (2018). Oligocene climate signals and forcings in Eurasia revealed by plant macrofossil and modelling results. Gondwana Research, 61, 115–127. https://doi.org/10.1016/j.gr.2018.04.015

715 Li, Y., Smith, T., Svetlana, P., Yang, J., Jin, J.-H., and Li, C.-S. (2014). Paleobiogeography of the lotus plant (Nelumbonaceae: Nelumbo) and its bearing on the paleoclimatic changes. Palaeogeography, Palaeoclimatology, Palaeoecology, 399, 284–293. https://doi.org/10.1016/j.palaeo.2014.01.022

Lunt, D. J., Bragg, F., Chan, W.-L., Hutchinson, D. K., Ladant, J.-B., Niezgodzki, I., Steinig, S., Zhang, Z., Zhu, J., Abe-Ouchi, A., de Boer, A. M., Coxall, H. K., Donnadieu, Y., Knorr, G., Langebroek, P. M., Lohmann, G., Poulsen, C. J.,
720 Sepulchre, P., Tierney, J., … Otto-Bliesner, B. L. (2020). DeepMIP: Model intercomparison of early Eocene climatic optimum (EECO) large-scale climate features and comparison with proxy data. Climate of the Past Discussions. https://doi.org/10.5194/cp-2019-149

Lunt, D. J., Farnsworth, A., Loptson, C., Foster, G. L., Markwick, P., O'Brien, C. L., Pancost, R. D., Robinson, S. A., and Wrobel, N. (2016). Palaeogeographic controls on climate and proxy interpretation. Climate of the Past, 12(5), 1181–1198.
725 https://doi.org/10.5194/cp-12-1181-2016

Madec, G. (2008). NEMO ocean engine (Note Du Pôle de Modélisation de l'Institut Pierre-Simon Laplace).

Marigó, J., Susanna, I., Minwer-Barakat, R., Madurell-Malapeira, J., Moyà-Solà, S., Casanovas-Vilar, I., Robles, J. M., and Alba, D. M. (2014). The primate fossil record in the Iberian Peninsula. Journal of Iberian Geology, 40(1), 157–166. https://doi.org/10.5209/rev_JIGE.2014.v40.n1.44094

730 Matthews, K. J., Maloney, K. T., Zahirovic, S., Williams, S. E., Seton, M., and Müller, R. D. (2016). Global plate boundary evolution and kinematics since the late Paleozoic. Global and Planetary Change, 146, 226–250. https://doi.org/10.1016/j.gloplacha.2016.10.002

Meng, J., and McKenna, M. C. (1998). Faunal turnovers of Palaeogene mammals from the Mongolian Plateau. Nature, 394(6691), 364–367. https://doi.org/10.1038/28603

735 Miller, K. G., Browning, J. V., Schmelz, W. J., Kopp, R. E., Mountain, G. S., and Wright, J. D. (2020). Cenozoic sea-level and cryospheric evolution from deep-sea geochemical and continental margin records. Science Advances, 6(20), eaaz1346. https://doi.org/10.1126/sciadv.aaz1346

Moraweck, K., Grein, M., Konrad, W., Kvaček, J., Kova-Eder, J., Neinhuis, C., Traiser, C., and Kunzmann, L. (2019). Leaf traits of long-ranging Paleogene species and their relationship with depositional facies, climate and atmospheric CO_2 level.
740 Palaeontographica Abteilung B, 298(4–6), 93–172. https://doi.org/10.1127/palb/2019/0062

Mosbrugger, V., Utescher, T., and Dilcher, D. L. (2005). Cenozoic continental climatic evolution of Central Europe. Proceedings of the National Academy of Sciences, 102(42), 14964–14969. https://doi.org/10.1073/pnas.0505267102

Mosbrugger, Volker, and Utescher, T. (1997). The coexistence approach—A method for quantitative reconstructions of Tertiary terrestrial palaeoclimate data using plant fossils. Palaeogeography, Palaeoclimatology, Palaeoecology, 134(1–4), 61–
745 86. https://doi.org/10.1016/S0031-0182(96)00154-X

Nott, J. F., and Owen, J. A. K. (1992). An Oligocene palynoflora from the middle Shoalhaven catchment N.S.W. and the Tertiary evolution of flora and climate in the southeast Australian highlands. Palaeogeography, Palaeoclimatology, Palaeoecology, 95(1–2), 135–151. https://doi.org/10.1016/0031-0182(92)90169-6

750 Page, M., Licht, A., Dupont-Nivet, G., Meijer, N., Barbolini, N., Hoorn, C., Schauer, A., Huntington, K., Bajnai, D., Fiebig, J., Mulch, A., & Guo, Z. (2019). Synchronous cooling and decline in monsoonal rainfall in northeastern Tibet during the fall into the Oligocene icehouse. Geology, 47(3), 203–206. https://doi.org/10.1130/G45480.1

PALAEOSENS Project Members. (2012). Making sense of palaeoclimate sensitivity. Nature, 491(7426), 683–691. https://doi.org/10.1038/nature11574

Pocknall, D. T. (1989). Late Eocene to early Miocene vegetation and climate history of New Zealand. Journal of the Royal
755 Society of New Zealand, 19(1), 1–18. https://doi.org/10.1080/03036758.1989.10426451

Pound, M. J., and Salzmann, U. (2017). Heterogeneity in global vegetation and terrestrial climate change during the late Eocene to early Oligocene transition. Scientific Reports, 7(1), 43386. https://doi.org/10.1038/srep43386

Prothero, D. R., and Heaton, T. H. (1996). Faunal stability during the Early Oligocene climatic crash. Palaeogeography, Palaeoclimatology, Palaeoecology, 127(1), 257–283. https://doi.org/10.1016/S0031-0182(96)00099-5

760 Quan, C., Liu, Y.-S. (Christopher), and Utescher, T. (2012). Paleogene temperature gradient, seasonal variation and climate evolution of northeast China. Palaeogeography, Palaeoclimatology, Palaeoecology, 313–314, 150–161. https://doi.org/10.1016/j.palaeo.2011.10.016

R Core Team (2020). R: A language and environment for statistical computing. R Foundation for Statistical Computing, Vienna, Austria. URL https://www.r-project.org/.

765 Rage, J.-C. (1986). The Amphibians and Reptiles at the Eocene-Oligocene Transition in Western Europe: An Outline of the Faunal Alterations. In Ch. Pomerol and I. Premoli-Silva (Eds.), Developments in Palaeontology and Stratigraphy (Vol. 9, pp. 309–310). Elsevier. https://doi.org/10.1016/S0920-5446(08)70135-3

Rage, J.-C. (2013). Mesozoic and Cenozoic squamates of Europe. Palaeobiodiversity and Palaeoenvironments, 93(4), 517–534. https://doi.org/10.1007/s12549-013-0124-x

770 Rasmussen, D. T., Brown, T. M., and Simons, E. L. (1992). The Eocene-Oligocene Transition in continental Africa. In D. R. Prothero and W. A. Berggren (Eds.), Eocene–Oligocene Climatic and Biotic Evolution (pp. 548–567). Princeton University Press.

Roček, Z., and Rage, J.-C. (2003). Evolution of anuran assemblages in the Tertiary and Quaternary of Europe, in the context of palaeoclimate and palaeogeography. Amphibia-Reptilia, 24(2), 133–167. https://doi.org/10.1163/156853803322390408

775 Saarinen, J., Mantzouka, D. and Sakala, J. (2020). Aridity, cooling, open vegetation, and the evolution of plants and animals during the cenozoic, in Nature Through Time, E. Martinetto, E. Tschopp, R. A. Gastaldo, Eds. (Springer Textbooks in Earth Sciences, Geography and Environment, Springer International Publishing), pp. 83–107.

Sagoo, N., Valdes, P., Flecker, R., and Gregoire, L. J. (2013). The Early Eocene equable climate problem: Can perturbations of climate model parameters identify possible solutions? Philosophical Transactions of the Royal Society A: Mathematical,
780 Physical and Engineering Sciences, 371(2001), 20130123. https://doi.org/10.1098/rsta.2013.0123

Scher, H. D., Bohaty, S. M., Smith, B. W., and Munn, G. H. (2014). Isotopic interrogation of a suspected late Eocene glaciation: Hidden glaciation revealed in the Eocene. Paleoceanography, 29(6), 628–644. https://doi.org/10.1002/2014PA002648

Sepulchre, P., Caubel, A., Ladant, J.-B., Bopp, L., Boucher, O., Braconnot, P., Brockmann, P., Cozic, A., Donnadieu, Y., Dufresne, J.-L., Estella-Perez, V., Ethé, C., Fluteau, F., Foujols, M.-A., Gastineau, G., Ghattas, J., Hauglustaine, D., Hourdin, F., Kageyama, M., … Tardif, D. (2020). IPSL-CM5A2 – an Earth system model designed for multi-millennial climate simulations. Geoscientific Model Development, 13(7), 3011–3053. https://doi.org/10.5194/gmd-13-3011-2020

Stehlin, H. G. (1909). Remarques sur les faunules de Mammifères des couches éocènes et oligocènes du Bassin de Paris. Société Géologique de France.

Stucky, R. K. (1992). In Eocene-Oligocene Climatic and Biotic Evolution (pp. 464–493). Princeton University Press. https://www.degruyter.com/princetonup/view/book/9781400862924/10.1515/9781400862924.464.xml

Sun, J., Ni, X., Bi, S., Wu, W., Ye, J., Meng, J., and Windley, B. F. (2015). Synchronous turnover of flora, fauna and climate at the Eocene–Oligocene Boundary in Asia. Scientific Reports, 4(1), 7463. https://doi.org/10.1038/srep07463

Tanrattana, M., Boura, A., Jacques, F. M. B., Villier, L., Fournier, F., Enguehard, A., Cardonnet, S., Voland, G., Garcia, A., Chaouch, S., and Franceschi, D. D. (2020). Climatic evolution in Western Europe during the Cenozoic: Insights from historical collections using leaf physiognomy. Geodiversitas, 42(11), 151–174. https://doi.org/10.5252/geodiversitas2020v42a11

Tardif, D., Fluteau, F., Donnadieu, Y., Hir, G. L., Ladant, J.-B., Sepulchre, P., Licht, A., Poblete, F., and Dupont-Nivet, G. (2020). The origin of Asian monsoons: A modelling perspective. Climate of the Past, 16(3), 847–865. https://doi.org/10.5194/cp-16-847-2020

Tardif, D., Toumoulin, A., Fluteau, F., Donnadieu, Y., Le Hir, G., Barbolini, N., Licht, A., Ladant, J.-B., Sepulchre, P., Viovy, N., Hoorn, C., & Dupont-Nivet, G. (2021). Orbital variations as a major driver of climate and biome distribution during the greenhouse to icehouse transition. *Science Advances*, 7(43), eabh2819. https://doi.org/10.1126/sciadv.abh2819

Teodoridis, V., & Kvaček, Z. (2015). Palaeoenvironmental evaluation of Cainozoic plant assemblages from the Bohemian Massif (Czech Republic) and adjacent Germany. *Bulletin of Geosciences*, 695–720. https://doi.org/10.3140/bull.geosci.1553

Tosal, A., Valero, L., Sanjuan, J., and Martín-Closas, C. (2019). Influence of short-and long-term climatic cycles on floristic change across the Eocene–Oligocene boundary in the Ebro Basin (Catalonia, Spain). Comptes Rendus Palevol, 18(8), 925–947. https://doi.org/10.1016/j.crpv.2019.10.003

Toumoulin, A., Donnadieu, Y., Ladant, J. -B., Batenburg, S. J., Poblete, F., and Dupont-Nivet, G. (2020). Quantifying the effect of the Drake Passage opening on the Eocene Ocean. Paleoceanography and Paleoclimatology. https://doi.org/10.1029/2020PA003889

Utescher, T., Bruch, A. A., Erdei, B., François, L., Ivanov, D., Jacques, F. M. B., Kern, A. K., Liu, Y.-S. (C.), Mosbrugger, V., and Spicer, R. A. (2014). The Coexistence Approach—Theoretical background and practical considerations of using plant fossils for climate quantification. Palaeogeography, Palaeoclimatology, Palaeoecology, 410, 58–73. https://doi.org/10.1016/j.palaeo.2014.05.031

Utescher, Torsten, Bondarenko, O. V., and Mosbrugger, V. (2015). The Cenozoic Cooling – continental signals from the Atlantic and Pacific side of Eurasia. Earth and Planetary Science Letters, 415, 121–133. https://doi.org/10.1016/j.epsl.2015.01.019

Wade, B. S., Houben, A. J. P., Quaijtaal, W., Schouten, S., Rosenthal, Y., Miller, K. G., Katz, M. E., Wright, J. D., and Brinkhuis, H. (2012). Multiproxy record of abrupt sea-surface cooling across the Eocene-Oligocene transition in the Gulf of Mexico. Geology, 40(2), 159–162. https://doi.org/10.1130/G32577.1

820   Wing, S. L. (1987). Eocene and Oligocene Floras and Vegetation of the Rocky Mountains. Annals of the Missouri Botanical Garden, 74(4), 748–784. JSTOR. https://doi.org/10.2307/2399449

Wolfe, J. A. (1992). 21. Climatic, Floristic, and Vegetational Changes near the Eocene/Oligocene Boundary in North America. In D. R. Prothero and W. A. Berggren (Eds.), Eocene-Oligocene Climatic and Biotic Evolution (pp. 421–436). Princeton University Press. https://doi.org/10.1515/9781400862924.421

825   Wolfe, J. A. (1993). A method of obtaining climatic parameters from leaf assemblages (p. 71). U.S. Geological Survey Bulletin 2040. https://doi.org/10.3133/b2040

Wolfe, J. A. (1994). Tertiary climatic changes at middle latitudes of western North America. Palaeogeography, Palaeoclimatology, Palaeoecology, 108(3), 195–205. https://doi.org/10.1016/0031-0182(94)90233-X

Yang, J., Spicer, R. A., Spicer, T. E. V., and Li, C.-S. (2011). 'CLAMP Online': A new web-based palaeoclimate tool and its
830   application to the terrestrial Paleogene and Neogene of North America. Palaeobiodiversity and Palaeoenvironments, 91(3), 163–183. https://doi.org/10.1007/s12549-011-0056-2

Zachos, J., Pagani, M., Sloan, L. C., Thomas, E., and Billups, K. (2001). Trends, Rhythms, and Aberrations in Global Climate 65 Ma to Present. Science, 292(5517), 686–693. https://doi.org/10.1126/science.1059412

Zanazzi, A., Judd, E., Fletcher, A., Bryant, H., and Kohn, M. J. (2015). Eocene–Oligocene latitudinal climate gradients in
835   North America inferred from stable isotope ratios in perissodactyl tooth enamel. Palaeogeography, Palaeoclimatology, Palaeoecology, 417, 561–568. https://doi.org/10.1016/j.palaeo.2014.10.024

Zanazzi, A., Kohn, M. J., MacFadden, B. J., and Terry, D. O. (2007). Large temperature drop across the Eocene–Oligocene transition in central North America. Nature, 445(7128), 639–642. https://doi.org/10.1038/nature05551

Zhang, R., Kravchinsky, V. A., and Yue, L. (2012). Link between global cooling and mammalian transformation across the
840   Eocene–Oligocene boundary in the continental interior of Asia. International Journal of Earth Sciences, 101(8), 2193–2200. https://doi.org/10.1007/s00531-012-0776-1

Zhu, J., Poulsen, C. J., and Tierney, J. E. (2019). Simulation of Eocene extreme warmth and high climate sensitivity through cloud feedbacks. Science Advances, 5(9), eaax1874. https://doi.org/10.1126/sciadv.aax1874

845

Simulation	$p\text{CO}_2$	AIS	%Land (Mkm²)	MAT (°C)	SST (°C)
4X	1120 ppm	/	132.3	26.4	28.2
3X*	**840 ppm**	**/**	**132.3**	**23.7**	**25.9**
2X	560 ppm	/	132.3	20.6	23.2
2X-ICE	560 ppm	$32.5 \times 10^6 \text{km}^3$	132.3	19.7	22.9
2X-ICE-SL*	**560 ppm**	**$32.5 \times 10^6 \text{km}^3$**	**152.7**	**18.7**	**22.2**

Table 1: Experimental design. Abbreviations: AIS: Antarctic Ice-Sheet volume (Ladant et al., 2014b); % Land: total land surface (millions of km²: 10^6km^2); MAT: Mean Annual global 2-meter air Temperature (°C); SST: Sea Surface Temperatures (°C). Simulations with an asterisk constitute realistic middle Eocene (Lutetian / Bartonian) and early Oligocene (Rupelian) scenarios, others are either sensitivity experiments (2X, 2X-ICE) or use the high value of the $p\text{CO}_2$ range estimated for the time interval (4X).

	2X - 4X	2X-ICE - 4X	2X-ICE-SL - 4X	2X - 3X	2X-ICE - 3X	2X-ICE-SL - 3X
Average ∆MATR model-data mismatch	-3.5°C	-3.9°C	-1.9°C	-2.8°C	-3.2°C	-1.2°C
RMSE	3.1°C	3.4°C	2.5°C	2.9°C	3.2°C	2.4°C
%	19.4%	19.4%	41.9%	22.6%	16.1%	45.2%
rho	0.21 (*p* = 0.28)	0.27 (*p* = 0.16)	0.29 (*p* = 0.12)	0.19 (*p* = 0.32)	0.25 (*p* = 0.20)	0.29 (*p* = 0.12)

Table 2: Priabonian-Rupelian data-model comparison. Negative mean ∆MATR values reflect a tendency of the model to underestimate ∆MATRs. The line "%" give the percentage of sites where the direction of ∆MATR is adequately modelled (e.g., the model described a MATR reinforcement in the zone where data indicate MATR increase). Modelled ∆MATR estimates were considered as positive when > 0.5, negative when < 0.5, or null when ranging [-0.5; 0.5]. "*rho*" indicates the strength of the correlation estimated with the Spearman Rank test, with associated p-values ("p"). Note that all p-values being > 0.05, none of the correlations are significant.
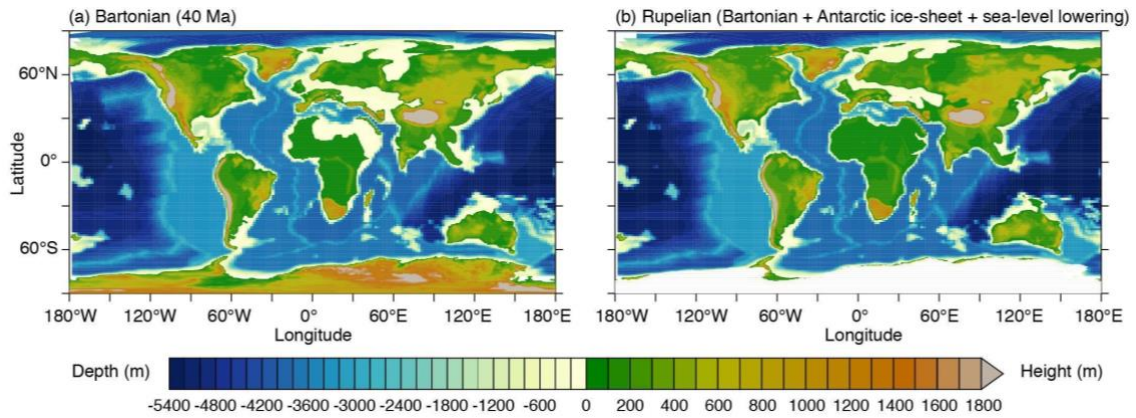
Figure 1: Paleotopographic 40 Ma map: (a) standard version as used for simulations 4X, 3X, 2X and 2X-ICE; (b) version adjusted with a homogeneous 70 m sea-level lowering used for the simulation 2X-ICE-SL (Poblete et al., *2021*).

865
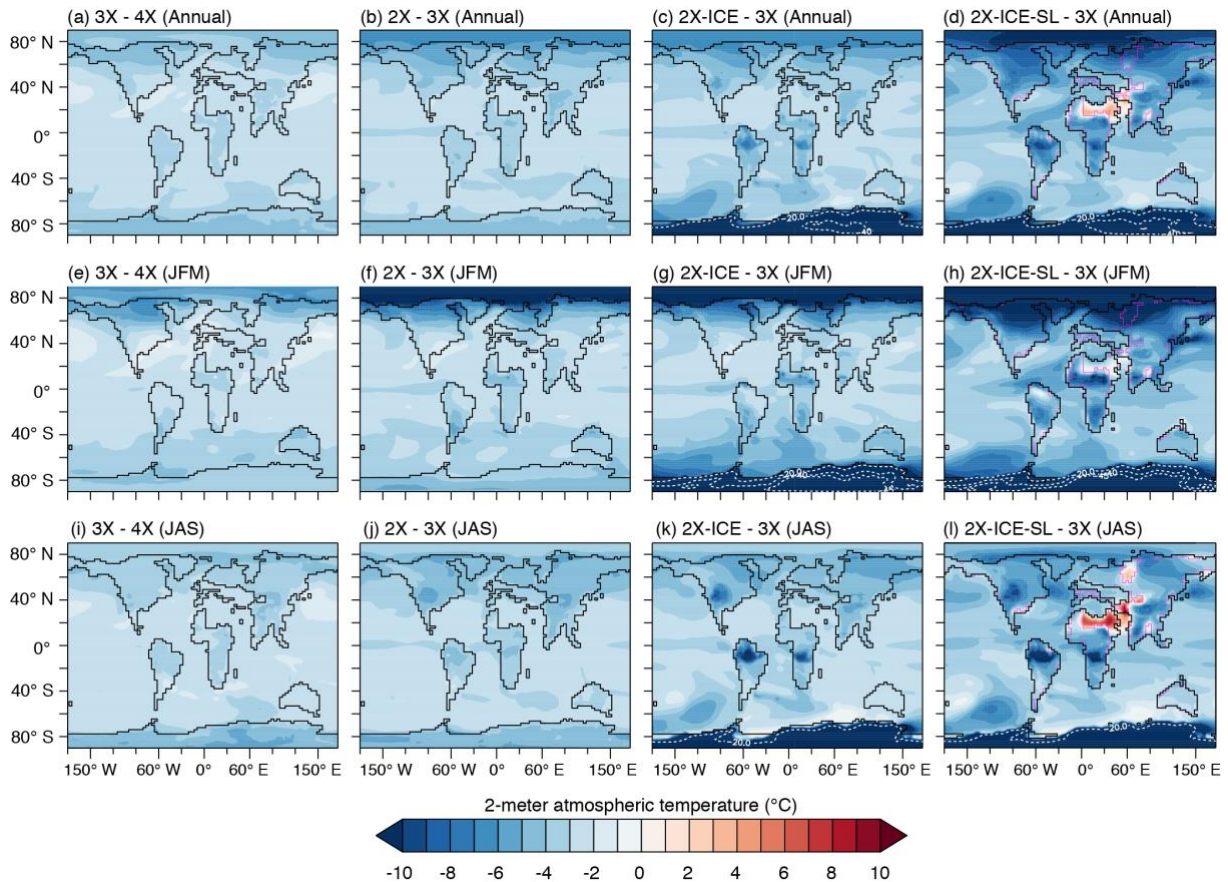
Figure 2: 2-meter air temperature changes (°C). JFM: averaged over January to March, JAS: averaged over July to September. Magenta lines of subfigures d,h,l indicate shorelines before sea-level lowering. White dotted lines in c,d,g,h,k,l are the level lines encircling the 20, 40 and 45°C cooling zones.
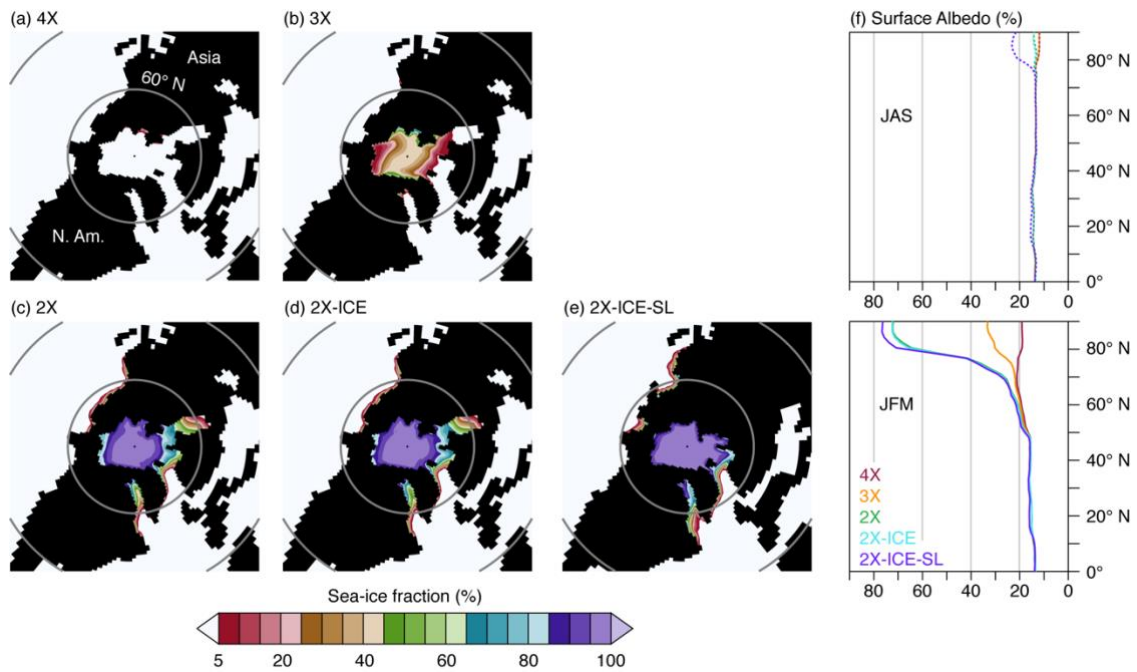
Figure 3: Northern Hemisphere winter sea-ice fraction and surface albedo (%)
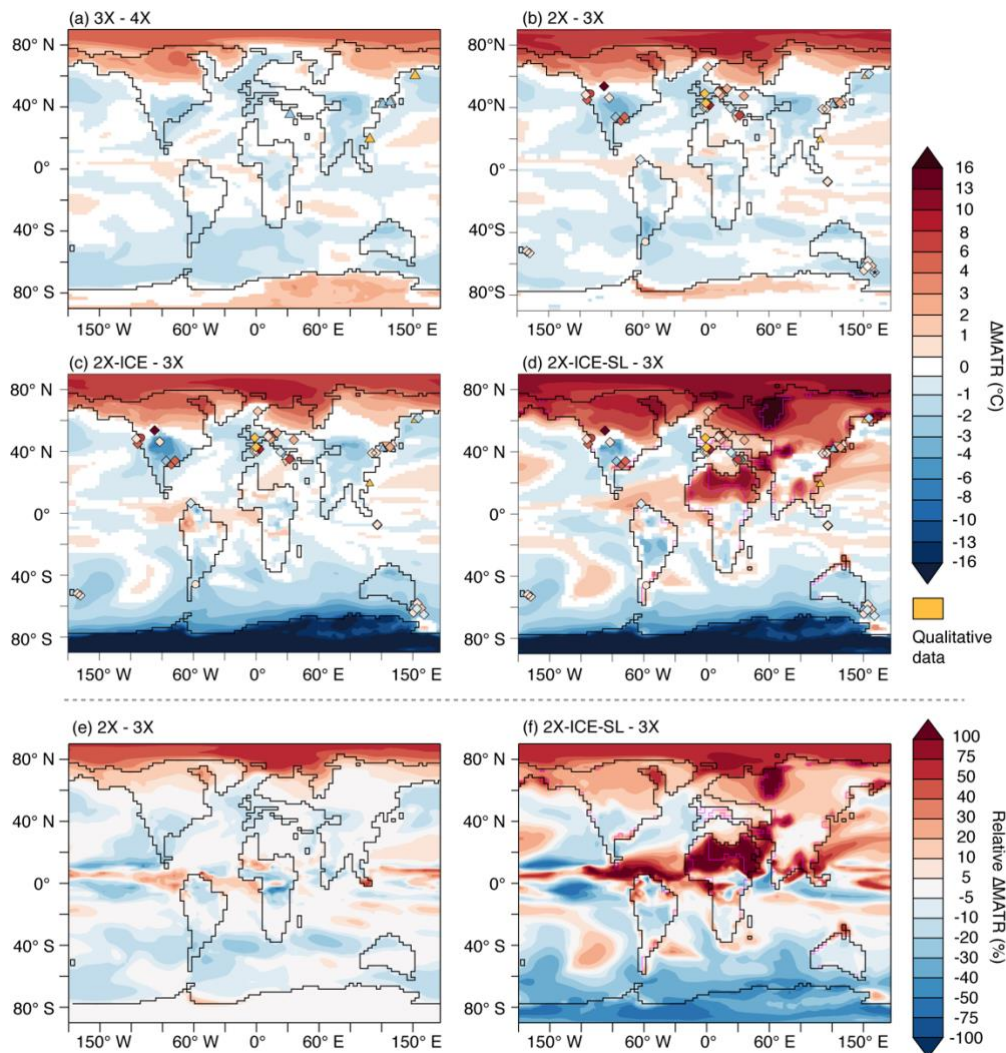
Figure 4: Changes in Mean Annual Temperature Range, ΔMATR (°C). Shadings are model differences calculated with a Student t-test over the last 100 years of comparative simulations (95% confidence); white areas indicate no significant ΔMATR. Subfigures e,f indicate relative ΔMATR (in %), for 2X-3X and 2X-ICE-SL - 3X respectively. Symbols correspond to ΔMATR from proxy-data for different time steps: Priabonian–Lutetian (triangles); Rupelian–Lutetian (deltas); Rupelian–Bartonian (circles); Rupelian–Priabonian (diamonds). Orange symbols indicate qualitative values describing a temperature seasonality increase. In case of proxies reconstructing a range of equally probable values (e.g., Coexistence approach), values shown are mean values. References are displayed on Figure 8 and available in the data compilation provided in Table S1.

875
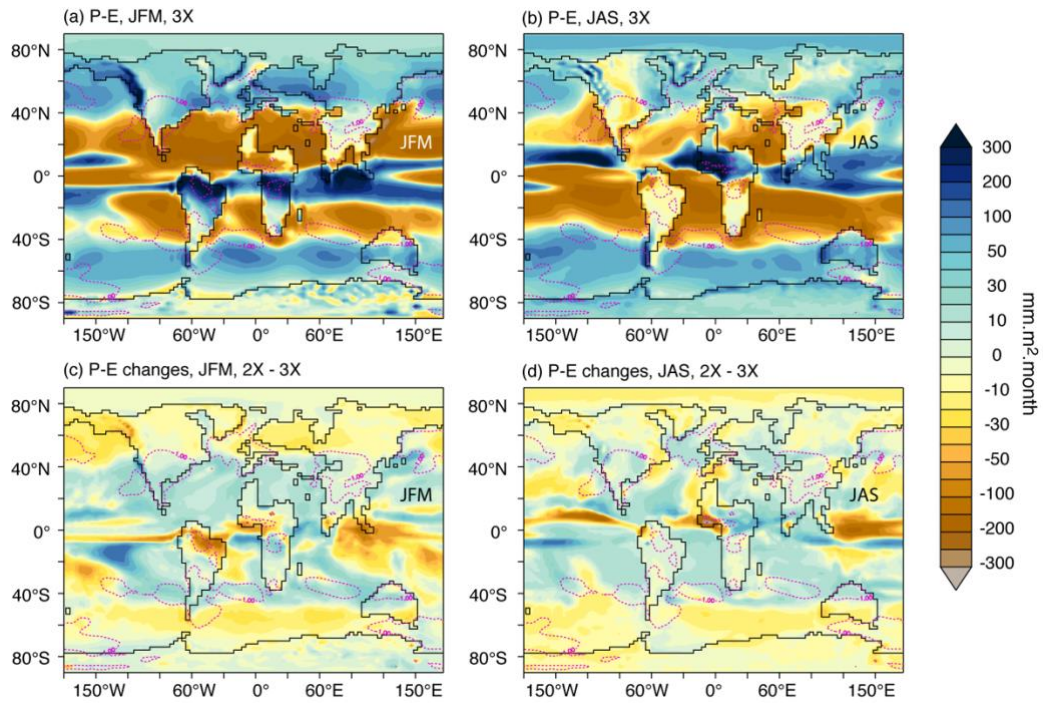
880

Figure 5: (a,b) Net precipitation (precipitation – evaporation, P-E) in JAS and JFM for the late Eocene simulation 3X. (c,d) Changes associated with pCO2 drop from 3X to 2X (differences shown are 2X *minus* 3X) for net precipitation. Magenta dashed lines contour areas with decreased seasonality (ΔMATR ≤ -1°C) in 2X *minus* 3X simulations (blue zones in Figure 4.b).
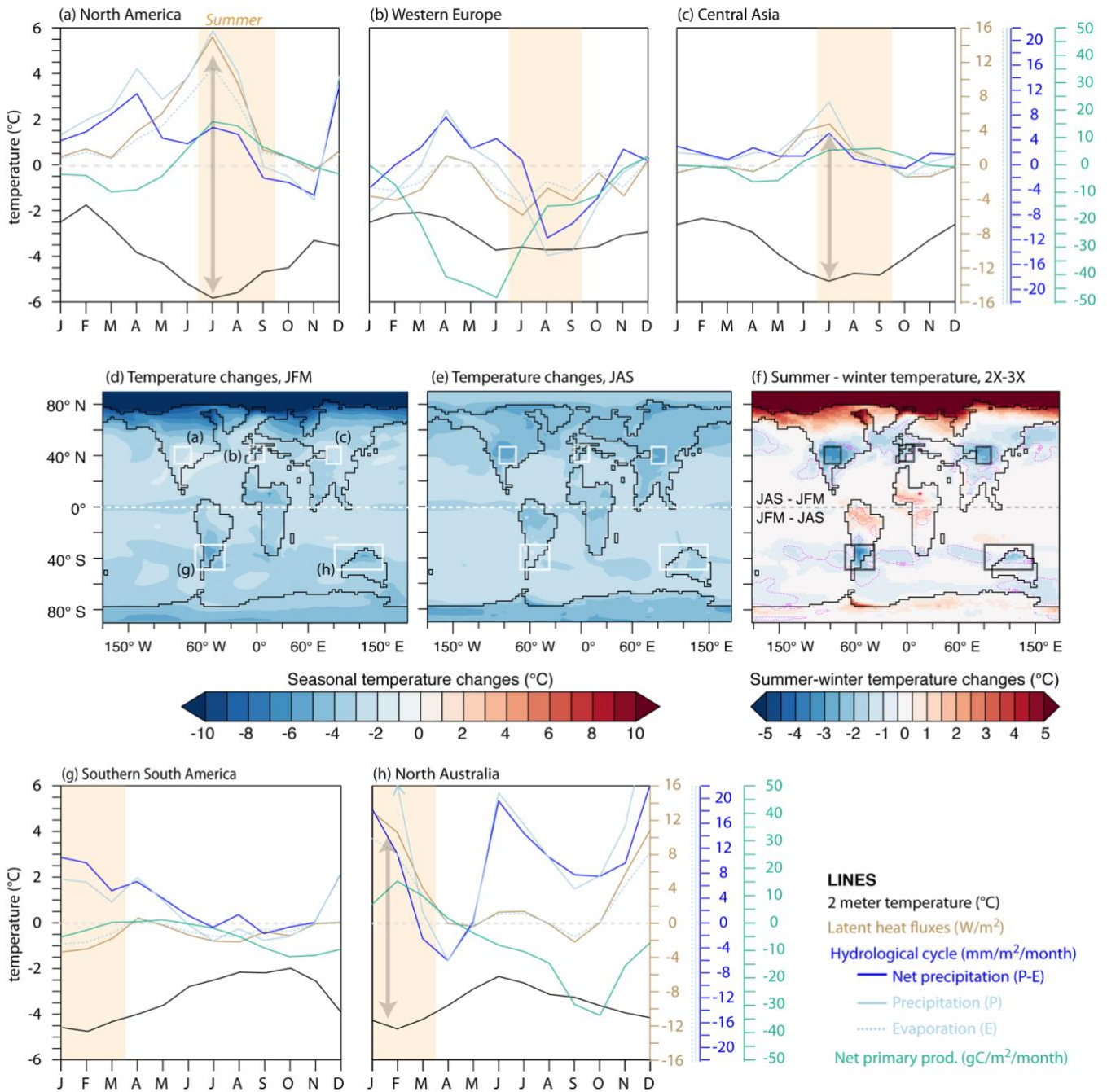
Figure 6: Annual variability of multiple climate parameters within the different areas of decreasing seasonality between 3X and 2X (a-c,g,h): atmospheric temperature (black), latent heat fluxes (soil to atmosphere; brown), hydrological cycle (incl. precipitation, evaporation and net precipitation, different shades of blue), and net primary productivity (green). (d-f) Temperature changes and summer *minus* winter temperature changes. Rectangles outline the land areas analysed in subfigures a-c,g,h (ocean zones are not taken into account in the calculation of the plots). Grey arrows show where decreasing summer temperatures match increased latent heat fluxes.
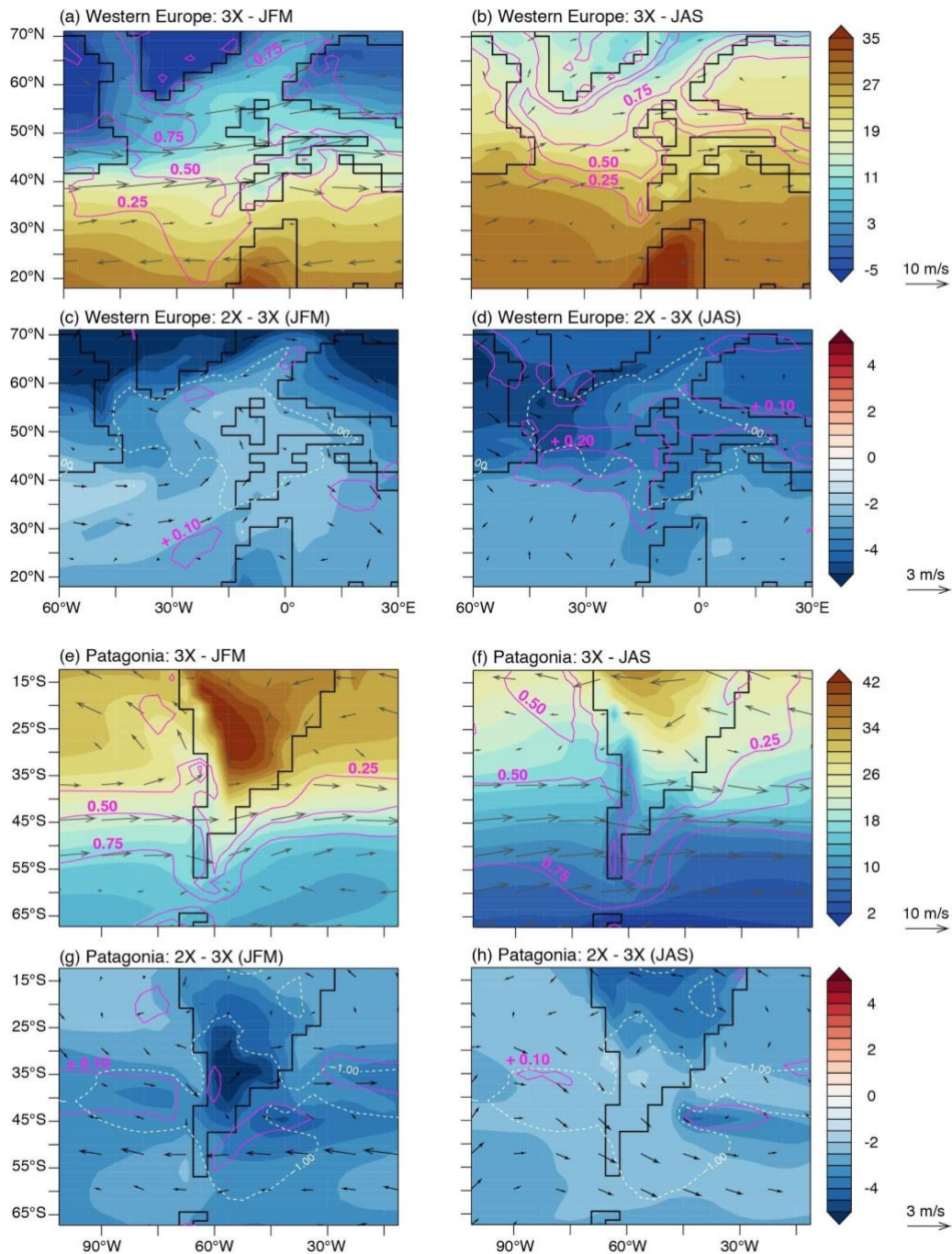
Figure 7: 2-meter atmospheric temperature across western Europe and Patagonia. Shadings correspond to temperatures (a,b,e,f) and temperature differences (c,d,g,h). Similarly, magenta lines contour low-level fraction (a,b,e,f) and low-level cloud fraction changes (c,d,g,h; always expressed in %) and arrows, 850 hPa winds (a,b,e,f) and 850 hPa wind changes (c,d,g,h; always in m.s^{-1}). White dashed lines contour areas with decreased seasonality (ΔMATR ≤ -1°C) in 2X *minus* 3X simulations (blue zones in Figure 4.b).
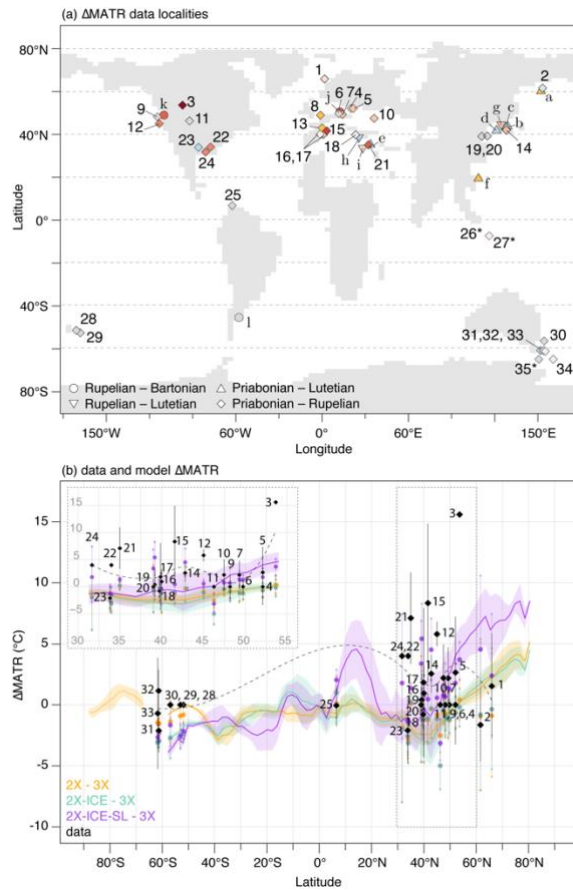
Figure 8: Data-model comparison of ΔMATR from the Priabonian to the Rupelian. (a). Map of all data ΔMATR estimates compiled in this study (symbols refer to the time period compared for the calculation of the MATR shift, see Table S1 for associated references). (b). Comparison of data estimates of Priabonian-Rupelian ΔMATR (black diamonds) to modelled ΔMATR at same localities (colored circles, calculated over a 3x3° area) from different pairs of simulations with 3X. Error bars are minimum and maximum data estimates of ΔMATR. Dashed black line is the LOESS curve associated to data ΔMATR estimates. Bold colored lines indicate the continental latitudinal gradient of ΔMATR on land (i.e., all longitudes averaged per degree of latitude); color-shaded intervals are the standard deviation around the average. A subfigure similar to (b) but using the simulation 4X as a Priabonian stage is available in supporting material, Fig. S9.